



REVIEW

Advances in high-temperature operatable triboelectric nanogenerator

Ruirui Cao^{1,2,3} | Ying Liu¹ | Huilin Li¹ | Zhitao Shen¹ | Fumin Li¹ |
Xiaoyong Jia¹ | Chong Chen^{1,4} | Rong Liu¹ | Caiqin Luo¹  | Wensheng Yang³ |
Rongrong Bao² | Caofeng Pan² 

¹Henan Key Laboratory of Photovoltaic Materials, School of Future Technology, Henan University, Kaifeng, China

²CAS Center for Excellence in Nanoscience, Beijing Key Laboratory of Micro-Nano Energy and Sensor, Beijing Institute of Nanoenergy and Nanosystems, Chinese Academy of Sciences, Beijing, China

³Engineering Research Center for Nanomaterials, Henan University, Kaifeng, China

⁴Institute of Solid State Physics, HFIPS, Chinese Academy of Sciences, Hefei, China

Correspondence

Chong Chen, Henan Key Laboratory of Photovoltaic Materials, School of Future Technology, Henan University, Kaifeng, China.

Email: chongchen@henu.edu.cn

Wensheng Yang, Engineering Research Center for Nanomaterials, Henan University, Kaifeng, China.

Email: wsyang@henu.edu.cn

Caofeng Pan, CAS Center for Excellence in Nanoscience, Beijing Key Laboratory of Micro-Nano Energy and Sensor, Beijing Institute of Nanoenergy and Nanosystems, Chinese Academy of Sciences, Beijing, China.

Email: cspan@binn.cas.cn

Abstract

The triboelectric nanogenerator (TENG) offers a novel approach to harness mechanical energy continuously and sustainably. It has emerged as a leading technology for converting mechanical energy into electricity. The demand for self-powered wearable microelectronics and energy generation in extreme conditions underscores the need for efficient high-temperature operatable TENGs (HTO-TENGs). However, the operating environment temperature not only affects the storage and dissipation of electrons during triboelectrification, leading to decreased output performance of TENG and instability at high temperatures, but also damage to the mechanical stability and effective defects in most tribo-materials, resulting in a further reduction in TENG's effective output power. Moreover, the unstable material properties of the triboelectric layer at high temperatures also restrict the use of the TENG in harsh environments. Therefore, it is imperative to consider the structural durability and electrical output stability of TENG when applying it in challenging working environments. This review aims to bridge this gap by providing a comprehensive overview of the current state and research advancements in HTO-TENG for the first time. Finally, this review presents insights into future research prospects and proposes design strategies to facilitate the rapid development of the field.

KEYWORDS

electrical output stability, harsh environments, high-temperature operatable, thermionic emission, triboelectric nanogenerator

Funding information: National Natural Science Foundation of China, Grant/Award Numbers: 52003074, 52125205, U20A20166, 52192614, 52003073, 62174049; China Postdoctoral Science Foundation, Grant/Award Number: 2020M680097; Postdoctoral Fellowship Program of CPSF, Grant/Award Number: GZC20230681; Natural Science Foundation of Henan Province, Grant/Award Number: 202300410058; National Science Fund for Excellent Young Scholars of Henan Province, Grant/Award Number: 222300420033; National key R&D program of China, Grant/Award Numbers: 2021YFB3200302, 2021YFB3200304; Natural Science Foundation of Beijing Municipality, Grant/Award Numbers: Z180011, 2222088; Shenzhen Science and Technology Program, Grant/Award Number: KQTD20170810105439418; Fundamental Research Funds for the Central Universities

This is an open access article under the terms of the [Creative Commons Attribution](https://creativecommons.org/licenses/by/4.0/) License, which permits use, distribution and reproduction in any medium, provided the original work is properly cited.

© 2024 The Author(s). *SusMat* published by Sichuan University and John Wiley & Sons Australia, Ltd.

1 | INTRODUCTION

As concerns about the depletion of fossil fuels and their impact on the environment continue to grow, researchers have been exploring renewable energy sources more fervently than ever before.¹⁻³ Finding sustainable energy sources from the surrounding environment to reduce carbon emissions, ensure long-term energy supply, and diminish dependence on fossil fuels has become an essential condition for the sustainable development of human civilization.⁴⁻⁷ Fortunately, the invention of triboelectric nanogenerator (TENG) in 2012, as an eco-friendly, enduring and self-sufficient power source, has opened up new possibilities for effective use of various forms of mechanical energy.⁸⁻¹⁰ Since invention, the number of TENG publications per year has significantly increased according to the analysis of published literature from the Web of Science database (Figure 1A). As a novel branch of energy conversion technology, TENG can efficiently convert the ubiquitous mechanical energy from the environment, including wind, vibration, water waves, biological energy, and human motion, into electrical energy through the coupling effect of contact electrification (CE) and electrostatic induction.^{11,12} Unlike traditional power sources, TENG boasts several unique advantages, including a simple structure (basically two contact materials and electrodes), ease of manufacturing, lightweight, flexibility, low cost, high efficiency even at low operation frequency, sustainability, and unrestricted material selection.¹³⁻¹⁷ As a result, TENG has the potential to revolutionize the way we power various devices and systems, including human motion monitoring, athletic big data analytics, biochemical detection, and wearable electronics.^{9,18-22} It is regarded as one of the most promising technologies to harvest electricity from mechanical kinetic energy, which will facilitate our transition toward a more sustainable future.

Currently, the majority of research in the field of TENG predominantly focuses on designing power supply systems or self-powered sensors within room temperature range.^{4,23-26} However, due to increasing demand for self-powered wearable microelectronics in scientific missions and energy production under extreme environments such as automotive engines, oil exploration, geothermal wells, industrial plants, military, wildfires, and aerospace electronics systems,^{27,28} efficient collection of triboelectric energy at high temperatures has become a crucial research area.^{29,30} Relevant research in this area is gradually emerging, as evidenced by the data extracted from Web of Science (Figure 1B). Nevertheless, the output performance of TENG is substantially influenced by ambient temperature, presenting new challenges.³¹⁻³⁴ Ensuring efficient and steady operation of TENG in a constantly changing environment is an urgent problem that needs to be addressed.

It is widely understood that the electron is the dominant CE transferred charge identity.^{24,35,36} The total surface charge output of TENG can be reasonably interpreted as the direct result of the coupling of the electron thermionic emission rate, the CE charge transfer rate, and the change in contact area between the two tribo-materials.^{24,37,38} Currently, TENG has been predominantly used to study CE at relatively low temperatures.^{4,23,39,40} However, at high temperatures, the electrostatic charge on the TENG surface can be released via electron thermionic emission and/or photon excitation.^{23,25,38,41} Consequently, the temperature of tribo-materials will affect the storage and dissipation of electrons in the process of triboelectrification, resulting in a decrease in the output performance of TENG and an inability to maintain a stable electrical output at high temperatures.⁴²⁻⁴⁴ Relevant studies have also further confirmed that increasing the tribo-layer's temperature will increase its electron thermionic emission rate, thereby

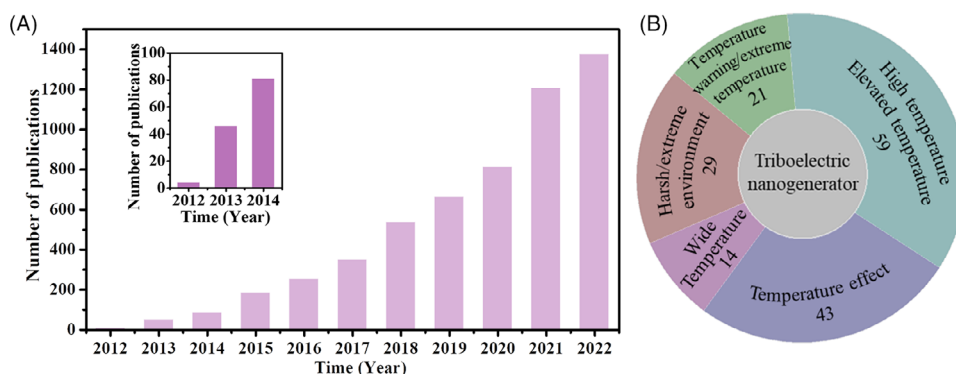


FIGURE 1 (A) The growth in the number of publications within the field of triboelectric nanogenerator (TENG) since its invention indicating of an increasing interest and investment in TENG research. (B) Summary of the publication count combing “triboelectric nanogenerator” with common terms related to the “high-temperature operable” in the June 2023 Web of Science search.

reducing the charge storage capacity of the tribo-layer and deteriorating TENG's output.^{27,44} Thermionic emission plays a critical role in explaining electron-dominated CE, where heating tribo-materials allows electrons to acquire sufficient thermal energy to overcome the work function and then emit from the tribo-materials.^{24,42,45} As there are limited studies on how to prevent or suppress this effect (thermionic emission), it is essential to further investigate its relationship with the operating environment temperature, as well as TENG output performance, in order to facilitate the development and application of high-temperature operable TENG (HTO-TENG) devices.

TENG is a highly effective technology for generating electricity from mechanical energy.^{33,46–48} Despite its many advantages, TENG's output can be negatively impacted by several factors. As mentioned above, the electron thermion emission rate of the tribo-layer increases as its temperature rises, which, in turn, reduces the charge storage capacity of the tribo-layer, ultimately leading to a decline in TENG's output.^{42–44} In addition to this issue, unstable material properties such as bandgap energy, interatomic bonding, breakdown field, carrier mobility, crystal structures, mechanical properties, and existing defects can also restrict the use of TENG in harsh environments.^{49,50} Moreover, exposure to high temperatures can cause damage to the mechanical stability and effective defects in most tribo-materials, resulting in a further reduction in TENG's effective output power.^{42,51} Therefore, it is essential to consider structural durability and electrical output stability when applying TENG technology in challenging working environments.^{4,45} To address these challenges, researchers are exploring new ways to enhance TENG's durability and expand its application fields.

As mentioned previously, in order to the efficient, stable, and continuous operation of tribo-materials in an environment with constantly changing conditions, it is necessary to prevent or suppress the electron thermionic emission effect and enhance structural stability at high temperatures. It is crucial for developing HTO-TENG and expanding its application fields. Despite being a thriving field, research progress on similar topics elsewhere has not been reviewed. This review aims to fill this gap by providing a comprehensive overview of the research progress and current situation in the field of HTO-TENG for the first time. The outline of this review is structured as follows: (1) Basic aspects of HTO-TENG are expounded, including the device's working mode, working mechanism, and temperature effect. (2) Recent advances in HTO-TENG are discussed from five different perspectives: device structure design, polymer-based tribo-materials structure design, gel-based TENG, carbon-based TENG, and metal-organic framework (MOF)-based TENG. (3) Prospects for future research are explored and some recommended design

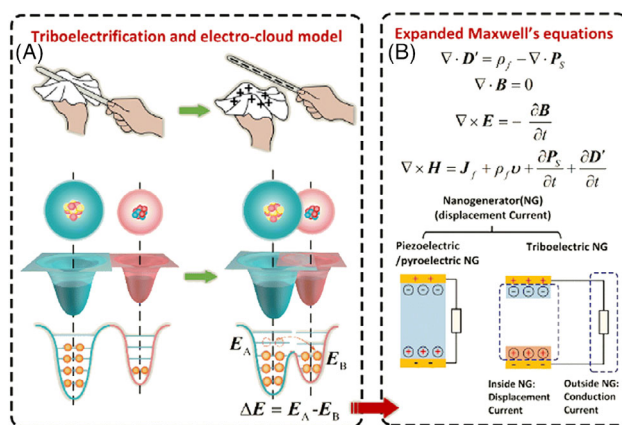


FIGURE 2 (A) Contact electrification and models of atomic potential energy and electronic states. (B) The augmented Maxwell's equations and the mechanism of NGs. *Source:* Reproduced with permission from Ref. [54]. Copyright 2022, The Royal Society of Chemistry.

strategies are proposed to facilitate the rapid advancement of this field.

2 | BASIC THEORY AND WORKING MECHANISM OF TENG

TENG efficiently converts ubiquitous mechanical energy in the environment into electricity through the coupling effect of CE and electrostatic induction.⁵² This section will delve into the fundamental theory, basic working mechanism and working modes, as well as the temperature effect of TENG.

2.1 | Contact electrification

The CE effect, also known as triboelectrification, is a fundamental phenomenon in electricity that involves the charge transfer between two dissimilar materials (Figure 2A), which is typically described as the ability of both materials to become charged during contact and separation.^{52–54} The emergence and rapid advancement of TENG technology have catalyzed fundamental research on CE. Prof. Wang put forward an electron-cloud overlap model that can explain the common occurrence of the CE effect in solid–solid and liquid–solid interfaces.^{23,55} Additionally, by utilizing the Kelvin probe force microscope system, Wang's team has investigated the fundamental mechanism of CE and concluded that electron transfer is the primary mechanism between solid–solid pairs.^{36,56–58} Specifically, the contact surfaces of two dissimilar materials generate equal electrostatic charges with opposite

polarity, and the separation of the two surfaces under an external force facilitates the contact-induced triboelectric charges to generate a potential drop, thereby driving electrons to flow between the two electrodes assembled on the top and bottom surfaces of the two materials.⁵⁹

2.2 | Maxwell's displacement current

Maxwell's equations, ranked among the top 10 equations in physics, hold immense significance in modern fundamental science and technologies.⁵⁴ To gain a deeper comprehension of TENG's working mechanism, Prof. Wang has proposed the formulation of Maxwell's displacement current for the TENG and its corresponding extended Maxwell's equations.^{55,59,60} In general, Wang's team has derived the differential form of the extended Maxwell's equations for a moving medium as a translational rigid object from the original differential form of Maxwell's equations for a fixed volume and boundary medium. Maxwell's equations for the moving charged medium (also known as the extended Maxwell's equations) are depicted in Figure 2B, where D' represents the displacement field, ρ_f represents the free electric charge density, B represents the magnetic field, E represents the electric field, H represents the magnetizing field, P_s represents the added term due to the presence of surface/volume electrostatic charges with the variation time in boundary shapes (independent of E), v represents the movement velocity of the medium, and J_f represents the free electric current density. Considering the presence of surface electrostatic charges resulting from CE, the invariant expressions of the modified equations under the action of displacement current are proposed. The extended Maxwell's equations make a significant contribution to the fundamental theory of TENG.^{60,61} To conclude, TENG utilizes the displacement current generated by external forces through the CE effect as a driving force to convert mechanical energy into electrical energy.

2.3 | Basic working modes of the TENG

Based on the coupling of two common phenomena, namely, CE and electrostatic induction, the basic working modes of TENG can be categorized into four modes (Figure 3): contact separation mode,^{44,51,62} single electrode mode,^{62–64} free-standing mode,^{25,65} and lateral sliding mode.^{24,66} Furthermore, TENGs can be categorized as contact and sliding mode based on the friction mode,^{67–70} as well as single or double dielectric-layered TENG depending on the number of dielectric layers.^{71,72} The four

working modes of TENG demonstrate distinct application scenarios due to variations in its structure and electrode arrangement.⁷³ In all instances, CE results in the generation of triboelectric charges with opposite polarities on the surface of materials. Subsequently, electrostatic induction produces a driving force that converts mechanical stimuli into electrical energy during relative motion.

2.4 | Temperature effect on performance of TENG

As previously mentioned, TENG is a novel energy conversion technology that utilizes the coupling effect of CE and electrostatic induction to convert mechanical energy into electrical energy.^{11,12} First, from the point of view of the tribo-charges, electron thermionic emission is the crucial factor that influences the fundamental mechanism of CE and is an inevitable effect in almost all tribo-materials.^{23,37} Electrons serve as the primary charge carriers in CE,^{23,24,37} which exhibits a strong temperature dependence (Figure 4A–F).²⁵ Specifically, electron thermionic emission poses a significant challenge at elevated temperatures (Figure 4G,H).²⁵ The overall surface charge output of the TENG can be attributed to the interplay between the electron thermionic emission rate, CE charge transfer rate, and the changing rate in contact area between the two materials.²⁴ Due to the electron thermionic emission effect, electrons transferred to the surface of the tribo-layer are released into the vacuum after CE,^{27,42} resulting in a reduction in surface charge density of the tribo-materials. Consequently, TENG cannot maintain effective output under high-temperature conditions. Second, from the perspective of the material, the intrinsic property of tribo-materials plays a crucial role in determining the output of TENGs.³¹ High temperatures not only induce changes in the dielectric constant of tribo-materials, which are closely linked to TENG's output performance,^{31,74} but also have the potential to cause structural and mechanical instability as well as material defects in most tribo-materials.^{75,76} As presented Figure 4I–M, exposure to elevated temperatures can result in unstable material properties, compromised mechanical durability and effective defects of most tribo-materials,^{4,31,42,49–51} thereby further diminishing the TENG's power output efficiency. In conclusion, the impact of high temperature on the output performance of TENGs needs to take into account multiple factors, including the surface charge density of tribo-materials, storage, and dissipation mechanisms for tribocharges, dielectric constant, structural stability, mechanical stability, and wear resistance.

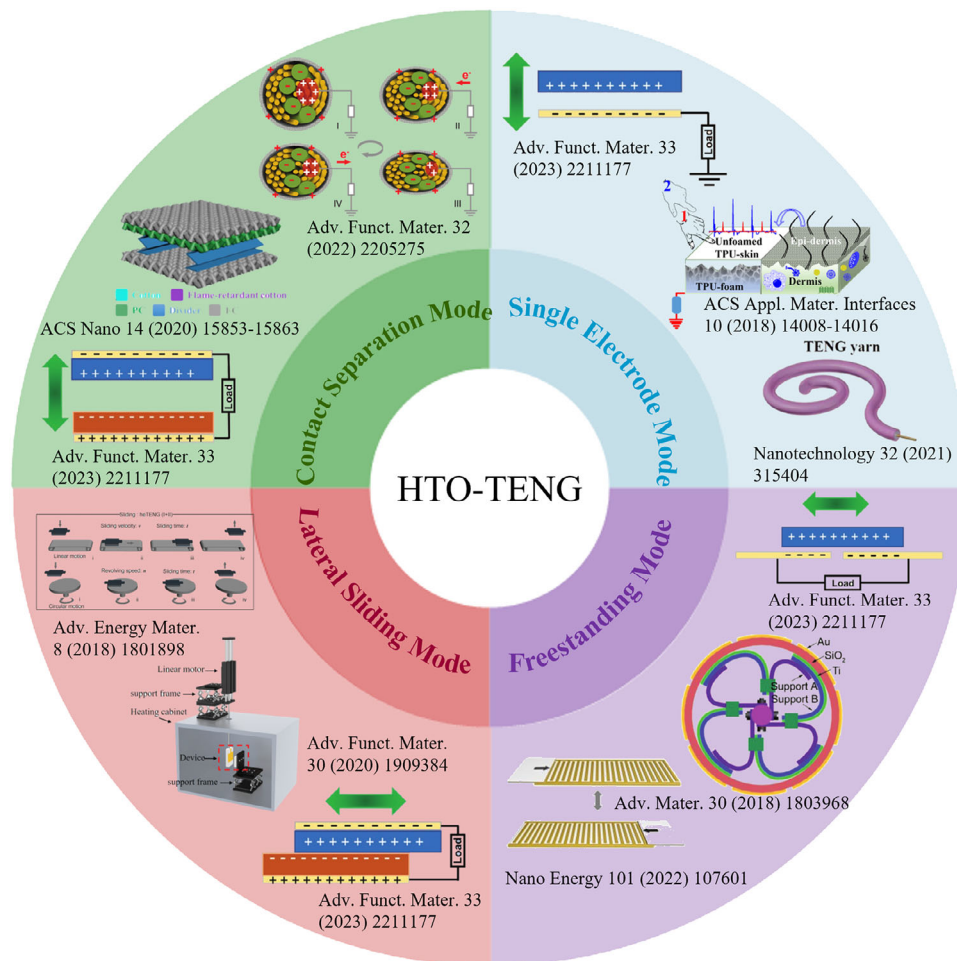


FIGURE 3 Fundamental modes of high-temperature operatable triboelectric nanogenerator (HTO-TENG) devices. *Source:* Reproduced with permission from Ref. [62]. Copyright 2023, Wiley-VCH. Reproduced with permission from Ref. [24]. Copyright 2020, Wiley-VCH. Reproduced with permission from Ref. [66]. Copyright 2018, Wiley-VCH. Reproduced with permission from Ref. [44]. Copyright 2020, American Chemical Society. Reproduced with permission from Ref. [51]. Copyright 2022, Wiley-VCH. Reproduced with permission from Ref. [63]. Copyright 2018, American Chemical Society. Reproduced with permission from Ref. [64]. Copyright 2021, IOP Publishing. Reproduced with permission from Ref. [25]. Copyright 2018, Wiley-VCH. Reproduced with permission from Ref. [65]. Copyright 2022, Elsevier.

3 | RECENT ADVANCES IN HTO-TENG

3.1 | Structural design of TENG devices

The strong temperature dependence of CE has been widely acknowledged, with electron thermionic emission being the main limiting factor of CE at high temperatures.^{24,25,42,45} A detailed investigation by Wen et al. examined the effect of temperature on TENG and confirmed that it could operate successfully at 500 K despite experiencing a significant drop in voltage due to thermionic emission.⁴³ To further broaden the operating temperature range of TENG devices, Xu et al. developed a polymer-free rotating self-standing mode TENG (R-TENG) with a double support structure made of spring steel and Al from a device structure design perspective, as shown in Figure 5A,B.²⁵ By optimizing this device structure, the R-

TENG with double supports achieved maximum output at 523 K, as displayed Figure 5D-F. Additionally, the working temperature of the R-TENG was increased to 673 K by suppressing thermionic emission through direct physical contact of the two support materials after preannealing, as shown in Figure 5D-F. The working mode, triboelectric materials, electrode, operating temperature, output performance, and output efficiency of this work and all below-mentioned works are listed in Table 1. This study successfully designed and constructed an R-TENG that was capable of operating up to 673 K, potentially broadening the temperature range of TENG applications to various extreme environments of planets, outer space, and even extrasolar planets.

In addition to the aforementioned support structure, the researchers have also developed a range of core-sheath TENGs capable of operating within a broad temperature

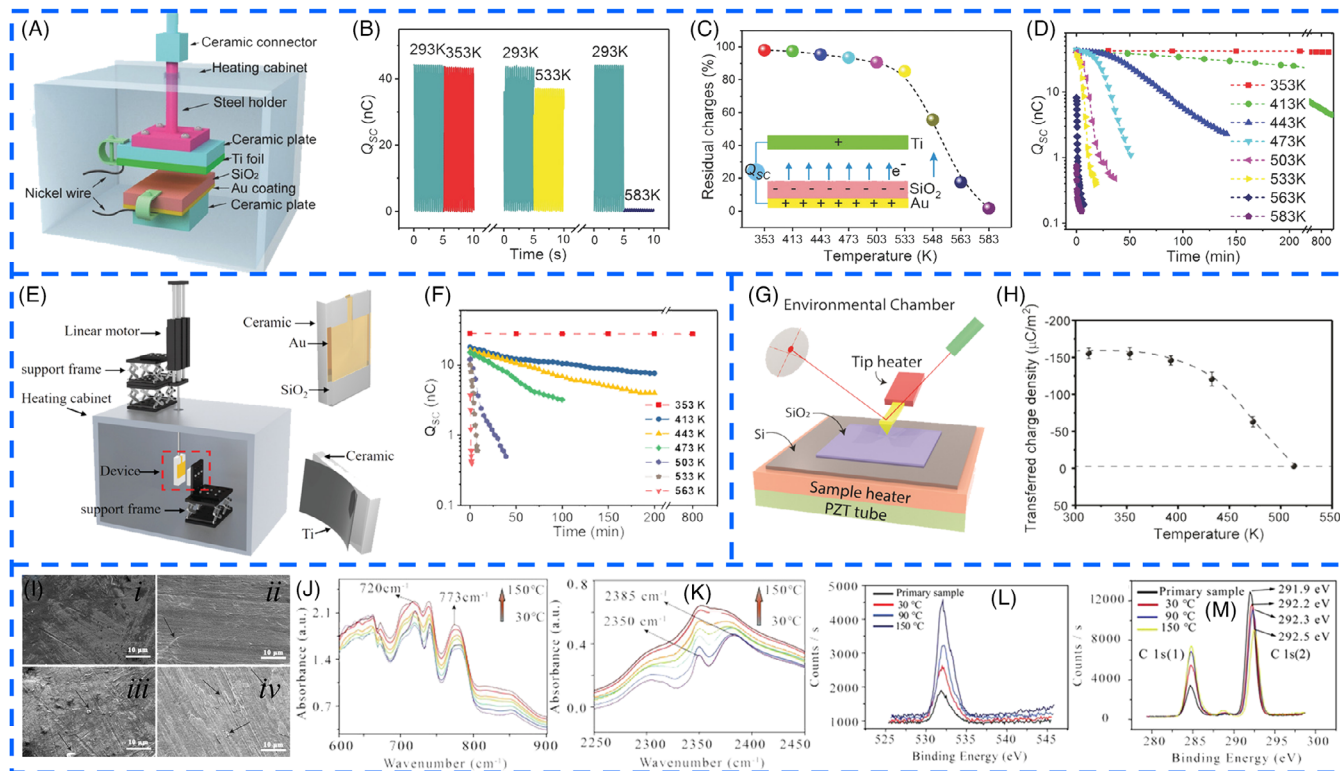


FIGURE 4 (A) Establishment of the measurement platform. (B) The measured transferred charges Q_{sc} at room temperature and different high temperatures. (C) The residual charge percentage of the triboelectric nanogenerator (TENG) at varying temperatures. (D) Q_{sc} thermal evolution over time. (E) Construction of the high-temperature measurement platform for TENGs. (F) Q_{sc} evolution over time at varying high temperatures. (G) Configuration of AFM experimental platform. (H) The temperature effect on the transferred charge density between the tip and SiO_2 sample. (I) SEM images of the polytetrafluoroethylene (PTFE) and flaking off thin sheets. The photos include (i-i) primitive PTFE without friction and the PTFE after 10 min of friction with an Al electrode at different temperatures: (i-ii) -20°C , (i-iii) 30°C , (i-iv) 150°C . The absorbance peak in the spectral regions of (J) $600\text{--}900\text{ cm}^{-1}$, (K) $2250\text{--}2450\text{ cm}^{-1}$. (L) The O 1s peak and (M) the C 1s peak under varying conditions. *Source:* (A–D) Reproduced with permission from Ref. [23]. Copyright 2018, Wiley-VCH. (E and F) Reproduced with permission from Ref. [24]. Copyright 2020, Wiley-VCH. (G and H) Reproduced with permission from Ref. [37]. Copyright 2019, Wiley-VCH. (I–M) Reproduced with permission from Ref. [4]. Copyright 2017, Wiley-VCH.

range.^{51,76–79} Zhong et al. created an innovative flexible, heat-resistant, and self-powered ionogel-based TENG (I-TENG) sensor featuring a core-sheath configuration, as depicted in Figure 5G.⁷⁶ The I-TENG comprises a double-network ionogel with excellent tensile and electrical conductivity as its electrode, aramid fibers serving as the tribo-positive layer, and a 3D-printed silicone sheath functioning as the tribo-negative layer. As exhibited in Figure 5H, the V_{oc} of I-TENG decreases with increasing temperature, resulting in a signal intensity reduction of approximately 30% at 200°C . Nonetheless, as illustrated in Figure 5I, although the maximum output signal of the I-TENG sensor initially decreases with increasing processing temperature and time, it eventually stabilizes. These results imply that although high temperature does affect voltage reduction to some extent, the stable output demonstrates that the sensor can still function efficiently even at 200°C . This is due not only to the superior thermal stability and triboelectric properties of the chosen tribo-materials

(double-network ionogel, aramid fibers, and silicone) but also to its unique core-sheath structure design. Xing et al. developed a highly flexible and long-lasting all yarns-based TENGs (Y-TENGs) with exceptional resistance to high temperatures.⁵¹ They accomplished this by utilizing a straightforward two-step doubling process that involved electrospinning and ancient twisting methods to incorporate silica aerogel into the polyimide (PI) nano-covered layer. The resulting multiply and stabilized triboelectric yarns were endowed with flame retardancy, heat insulation, and high-temperature resistance. As displayed in Figure 5J, the single triboelectric yarn possessed excellent flexibility and fineness and was wrapped around conductive spiral fiber bundles through a nano-covered electrospinning to form a tightly packed core-sheath structure. The produced triboelectric yarn was subjected to different temperatures on an electromagnetic heating plate, and the corresponding electrical output performance of Y-TENG is depicted in Figure 5K–M. From the figures, it

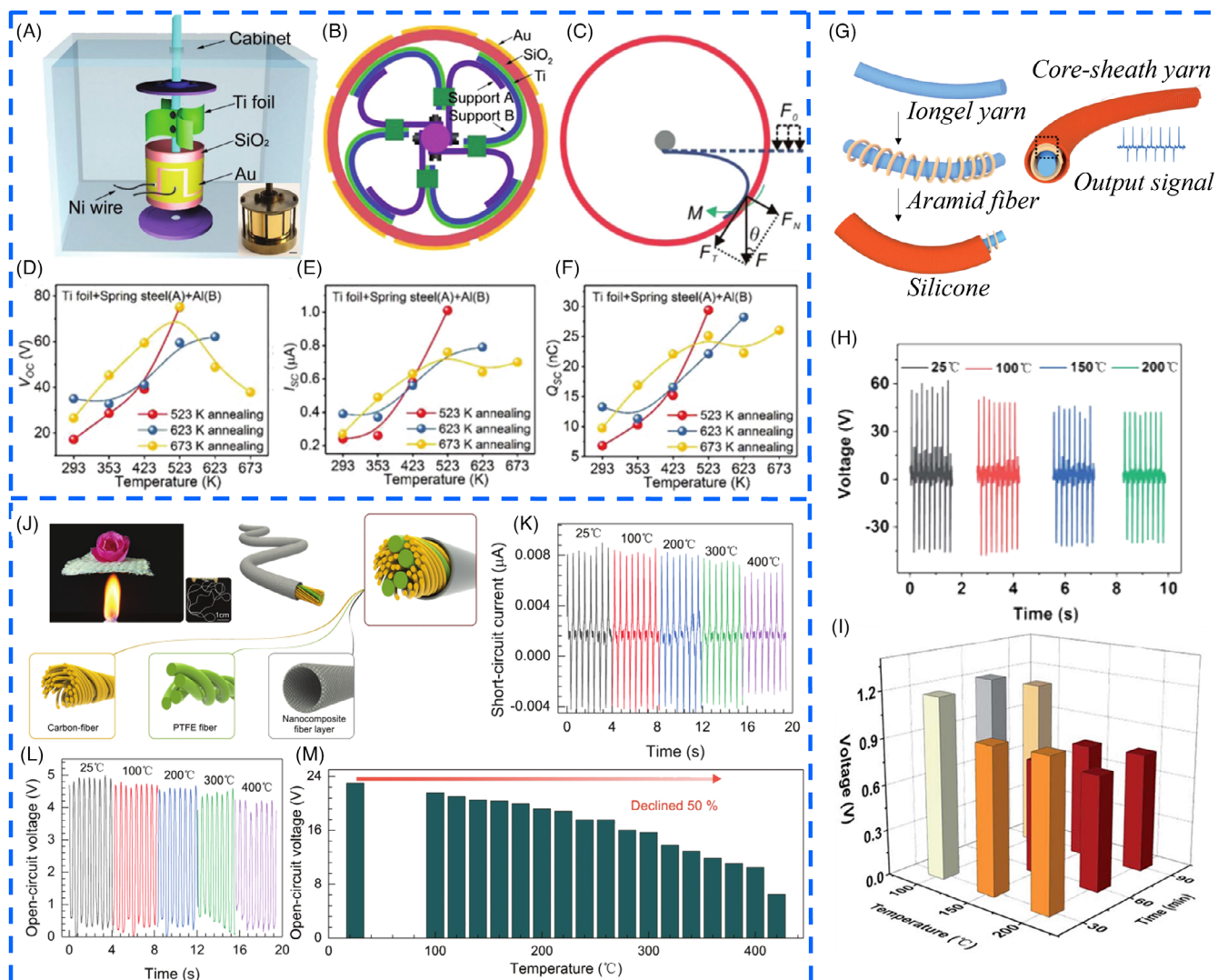


FIGURE 5 (A) Schematic illustration of the rotating self-standing mode triboelectric nanogenerator (R-TENG) in the high-temperature measurement platform. Inset is an optical photograph of the R-TENG. (B) Schematic diagram of the double support R-TENG. (C) Simplified mechanical model of the R-TENG structure. (D–F) V_{oc} , I_{sc} , and Q_{sc} of the R-TENG with an Al sheet as support A after annealing at various temperatures. (G) The assembly procedure and schematic diagram of the iongel-based TENG (I-TENG). (H) V_{oc} of I-TENG sensors under varying temperatures. (I) V_{oc} of the I-TENG with consistent bending angles at varying temperatures handled for varied times. (J) Schematic illustration of aerogel nano-coated triboelectric yarns. (K and L) I_{sc} and V_{oc} of triboelectric yarns at varying high temperatures. (M) V_{oc} of yarns-based TENG (Y-TENG) under different temperature conditions. *Source:* (A–F) Reproduced with permission from Ref. [25]. Copyright 2018, Wiley-VCH. (G–I) Reproduced with permission from Ref. [76]. Copyright 2022, The Royal Society of Chemistry. (J–M) Reproduced with permission from Ref. [51] Copyright 2022, Wiley-VCH.

can be observed that the electrical output performance of Y-TENG decreased slowly at the initial stage of heating but significantly worsened when the temperature surpassed 400°C. This indicates that the triboelectric yarn maintained good electrical output within the operating temperature range of 25–400°C, and the upper limit temperature was considerably raised when using prepared triboelectric yarns for fabricating Y-TENGs. This significant breakthrough in organic tribo-materials' temperature upper limit has the potential to improve the working temperature of textile-based TENG devices, thereby holding

enormous application prospects for energy generation and motion detection in high-temperature and other high-risk environments.

3.2 | Structural design of TENG PTMs

TENG is an innovative energy harvesting technique that combines CE and electrostatic induction effect to offer several advantages, including low-cost, high-power output, and superior energy conversion efficiency.^{80–82}

TABLE 1 A summary of triboelectric materials and output performance of high-temperature operatable (HTO)-triboelectric nanogenerators (TENGs) at various temperatures.

Section of this article	Working mode	Triboelectric materials	Electrode	Operating temperature	V_{oc}/I_{sc}	χ (%)	Ref.
3.1	Rotating free-standing mode with double supports	Ti and SiO ₂	Au	523 K	286 V	414	25
3.1	Single electrode mode	Aramid fiber and Silicone	Double-network ionogel	200°C	48 V	70	76
3.1	Single electrode mode	Silica aerogel/PI nanocomposite and PTFE	Carbon fiber	100°C	21.6 V	93.5	51
				200°C	19.2 V	83.1	
				300°C	15.7 V	66.2	
				400°C	10.6 V	45.9	
3.2.1	Flutter-driven single electrode mode	1% BaTiO ₃ -doped 6FDA-TFDB	Al	200°C	0.7 μ A	32	42
3.2.2	Single electrode mode	md-PI_95	Al	60°C	157 V	224	106
				70°C	127 V	181	
3.2.2	Contact separation mode	Cu/hc-PI	Cu	60°C	61 V	244	105
				70°C	58 V	232	
3.2.3	Contact separation mode	PVA/PPA-PEI and PVDF	Al	100°C	10.6 V	54.3	115
3.2.3	Single electrode mode	IAFE-25 and FEP	6AFE-26	200°C	27.3 V	120	116
				250°C	28.2 V	124	
3.2.3	Single electrode mode	EFM	Conductive elastic fabric	70°C	110 V	100	120
3.2.3	Single electrode mode	PH-SA film	Cu	60°C	117.8 V	285.3	121
				90°C	87.7 V	256.0	
				100°C	81.0 V	231.4	
3.2.3	Single electrode mode	Flame-retardant wood	Cu	200°C	–	82.0	18
				250°C	–	60.5	
3.2.3	Single electrode mode	CNF-BP-PA	CNF-BP-PA/AgNWs	80°C	129 V	131.6	142
				110°C	93 V	94.9	
3.3	Free-standing mode	Cu and PU	Cu	40°C	20.8 V	105	149
				55°C	23.8 V	120	
				70°C	56.1 V	282	
				85°C	58.6 V	294	
				100°C	61.4 V	309	
3.4	Contact separation mode	Cotton fibers and PTFE	Al	60°C	204 V	93.6	154

(Continues)

TABLE 1 (Continued)

Section of this article	Working mode	Triboelectric materials	Electrode	Operating temperature	V_{oc}/I_{sc}	χ (%)	Ref.
3.4	Contact separation mode	Flame-retardant conductive fabric and PTFE-coated fabric	Flame-retardant conductive fabric	100°C	75.2 V	73.0	44
				160°C	51 V	50.4	
				200°C	39.8 V	38.9	
				220°C	35.8 V	34.5	
3.4	Contact separation mode	Cu and PINF	Cu	100°C	49.3 V	80.8	45
				150°C	40.4 V	65.0	
				200°C	29.7 V	47.4	
				250°C	16.0 V	26.2	
3.5.1	Contact separation mode	Hydrogel and FEP	Ag NWs	40°C	10 V	100	165
3.5.1	Single electrode mode	Silicone rubber	Hydrogel	60°C	275 V	95.8	166
3.5.1	Single electrode mode	VHB	CPH	60°C	41 V	100	167
3.5.1	Single electrode mode	Commercial PU tape	MMCOHs	60°C	56.3 V	96.7	169
3.5.1	Single electrode mode	PAZ	PAAm-clay-KI organohydrogel	80°C	136 V	105	170
3.5.1	Single electrode mode	IU-PDMS	Paam-clay organohydrogel	80°C	154 V	100	171
3.5.1	Single electrode mode	SR	AVN organohydrogel	100°C	141 V	98.4	172
3.5.1	Single electrode mode	NSO	CSO	80°C	30 V	214	173
3.5.2	Single electrode mode	PDMS	Ionogel	60°C	4.35 μ A	106	184
3.5.2	Single electrode mode	Electrospun PVDF/PU	ICL	80°C	179 V	100	114
3.5.2	Single electrode mode	PDMS	Ionogel	100°C	111 V	100	186
3.5.2	Single electrode mode	RD-PDMS	TEOA-PTA@LiTFSI	60°C	82 V	115	188
3.5.3	Contact separation mode	SFS e-textile and PTFE fabric	Cu	150°C	1.98 V	53.1	194
				250°C	1.48 V	47.7	
3.5.3	Contact separation mode	PEO and PBO	ITO	350°C	32 V	100	195

Note: χ : Output efficiency;

$$\chi = \frac{V_T}{V_{Tmax}} \left(\frac{I_T}{I_{Tmax}} \right) \times 100\%$$

Abbreviations: CNF, cellulose nanofiber; CPH, cellulose/ polyvinyl alcohol hydrogel; EFM, electro-spun fiber membrane; NSO, nonconductive self-healable organohydrogels; PA, phytic acid; PBO, poly(*p*-phenylene benzobisoxazole); PINF, polyimide nanofiber; PTFE, polytetrafluoroethylene.

Typically, at least one of the triboelectric surfaces used in TENG is composed of a polymer material,^{83,84} such as polyvinylidene fluoride (PVDF),^{85,86} PI,^{13,87} nylon,^{88,89} polyacrylonitrile,^{90,91} and polytetrafluoroethylene.^{92,93} Compared to classical metal and inorganic tribo-materials, polymer tribo-materials (PTMs) possess various functional groups (–F, –CN, –COOH, and –CONH), which can facilitate charge transfer and capture during the CE process through their unique hybrid orbital configurations.^{8,94,95} Furthermore, PTMs also offer numerous advantages, including diverse material selection, excellent flexibility, processability, extensibility, ductility, and lightweight, making them the fundamental building blocks of TENG technology.^{8,96}

3.2.1 | Chemical structure design of PTMs

Thermionic emission plays a crucial role in the basic mechanism of CE, and it is an inevitable phenomenon for nearly all tribo-materials.^{23,37,42} During the CE process, electrons transferred to the tribo-surface can be thermally excited and escape into vacuum, thereby hindering the generation of tribo-charges and the energy output from TENG.⁹⁷ It is widely recognized that the thermionic emission effect imposes a significant restriction on high-temperature TENG, with tribo-charges typically being dismissed above 200°C.^{25,27,37} Consequently, the TENG cannot maintain effective electrical output in high-temperature environments. To address this issue and achieve high thermal charge stability, Tao et al. designed fluorinated PI (F-PI) films with exceptional charge thermal stability and high charge density by introducing strong electron-absorbing groups such as trifluoromethyl (–CF₃) and sulfone (–SO₂–) into the polymer backbone using chemical structure design techniques for PTMs themselves (Figure 6A).⁴² These F-PI films contain robust electron-absorbing groups in their backbone, which can provide a significant highest occupied molecular orbital and the lowest unoccupied molecular orbital and numerous surface states for charge transfer. The F-PI film, characterized by a large band gap, exhibits a remarkable tribo-charge density of 170 $\mu\text{C m}^{-2}$, which is four times higher than that of ordinary Kapton film.^{98,99} Additionally, the incorporation of BaTiO₃ nanofillers into the F-PI matrix can induce interfacial polarizations and electron deep traps, further enhancing the tribo-charge density (200 $\mu\text{C m}^{-2}$) and thermal charge stability of the tribo-polymer.^{43,100} Based on this BaTiO₃-doped F-PI film, Tao et al. developed a flutter-driven TENG (FD-TENG, Figure 6B) for wind energy harvesting and high-temperature wind speed detection. The FD-TENG demonstrated exceptional thermal charge stability, maintaining 32% output performance

at 200°C compared with room temperature (Figure 6C–G). This represents the highest reported thermal charge stability for the triboelectric polymer at the time; however, there still remains a concern regarding performance degradation in frictional electric output under elevated temperatures. This BaTiO₃-doped F-PI has great potential for application in self-powered sensors operating in hot air tunnels and other harsh environments, while also providing a viable strategy for harvesting environment energy under high-temperature conditions.

The emergence of TENG provides a secure approach to acquire eco-friendly energy and convert it into electrical power. Polymer-based TENGs, in particular, have shown great potential for powering flexible electronic devices without the need for external power sources. However, the majority of polymer materials utilized in TENG manufacturing are flammable and susceptible to melting and dripping when exposed to temperatures up to 220°C. This not only severely restricts the application of TENG under extreme conditions but also poses a significant risk to human health and safety.^{44,101,102} Advancements in design principles of material structure have significantly influenced the development of high-performance materials for future applications.²⁰ To address these challenges, researchers have explored new approaches to designing high-performance TENG materials with enhanced flame-retardant properties. For example, Guan et al. have ingeniously crafted a flame-retardant TENG by means of a one-pot melt polycondensation reaction, utilizing the all-aromatic liquid crystal poly(aryl ether ester) (LCP_{AEE}) as their base material (Figure 6H,I).²⁰ The high rigidity main chain of LCP_{AEE} not only endows the LCP-TENG with outstanding anti-dripping and temperature-resistance properties but also helps improve its fire-resistance characteristics.^{103,104} Moreover, the synthesized LCP-TENG demonstrates exceptional electrical output performance thanks to the high dielectric constant of LCP_{AEE} ($\epsilon' = 4.8$) and fibrous-structured morphology (Figure 6I). Even under extreme conditions, such as combustion at $\approx 520^\circ\text{C}$ for 16 s (Figure 6J,K), the LCP-TENG device exhibits remarkable resilience by maintaining an open-circuit voltage of over 65%. Furthermore, when connected to a bridge rectifier (Figure 6L), the LCP-TENG ($2 \times 2 \text{ cm}^2$) can power LED bulbs adorned with seabird patterns in a vivid green hue. Impressively, this light remains visible even after 16 s of combustion, demonstrating that LCP_{AEE} is capable of delivering stable electrical output performance under extreme environments (Figure 6M). These results suggest that the LCP-TENG holds immense potential in the realm of personal protective equipment, encompassing fire-resistant energy harvesters and rescue systems for use in extreme environments such as firefighting.

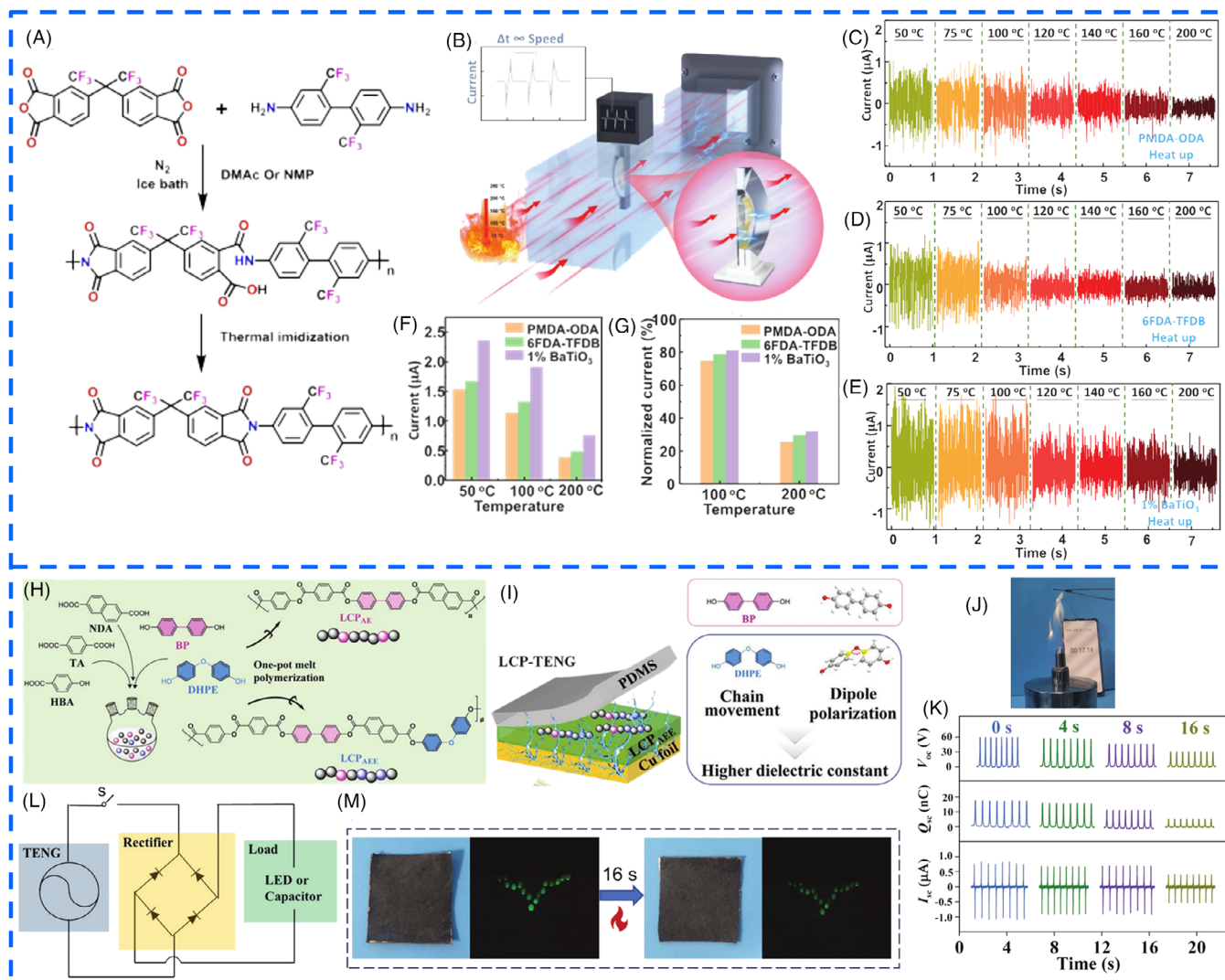


FIGURE 6 (A) Chemical synthesis of polyimides film (e.g., 6FDA-TFDB). (B) Schematic diagram of a high-temperature wind energy harvesting flutter-driven triboelectric nanogenerator (FD-TENG). The current of FD-TENG with (C) PMDA-ODA, (D) TFDB-6FDA, and (E) 1% BaTiO_3 -doped 6FDA-TFDB flaps. The current (F) and normalized current (G) of FD-TENG under varying temperatures. (H) Backbone composition of LCP_{AEE} with the introduction of DHPE into LCP_{AE} . (I) The design of LCP-TENG with intrinsic flame-retardancy. (J) The image of the combustion of triboelectric polymers in a flame. (K) The V_{oc} , Q_{sc} , and I_{sc} of LCP_{AEE} -TENG after burning for 4, 8, and 16 s, respectively. (L) The circuit diagram of charging system. (M) Photograph depicting the illumination of 17 LEDs pre- and postexposure to a 16-s burn-in period. *Source:* (A–G) Reproduced with permission from Ref. [42]. Copyright 2021, Wiley-VCH. (H–M) Reproduced with permission from Ref. [20]. Copyright 2022, Wiley-VCH.

3.2.2 | Physical structure design of PTMs

Polymer materials have a reputation for being vulnerable in harsh environments, particularly under high-temperature conditions.^{41,105} This is especially relevant when it comes to dielectric materials used in the production of typical TENG, as they are often made up of polymer films.^{83,84} In addition to the chemical structure design of PTMs mentioned above, the special physical structure design of tribo-materials can also enhance their heat resistance and high-temperature electrical output performance to some extent. As depicted in Figure 7,

Bui's team has developed highly efficient PI tribo-surfaces with customizable non-close packed microdome arrays (md-PI) and customizable honeycomb patterns (hc-PI) respectively.^{105,106}

Specifically, as illustrated in Figure 7A–C, Bui et al. developed an improved phase separation (IPS) method to imprint microdome pattern arrays on the surface of PI.¹⁰⁶ This results in the construction of a microdome-patterned PI (md-PI) with customizable non-close packed microbead arrays, which enhances the effective contact surface area and contact stress while taking advantage of the high thermal and mechanical stability of PI. The md-PI-based

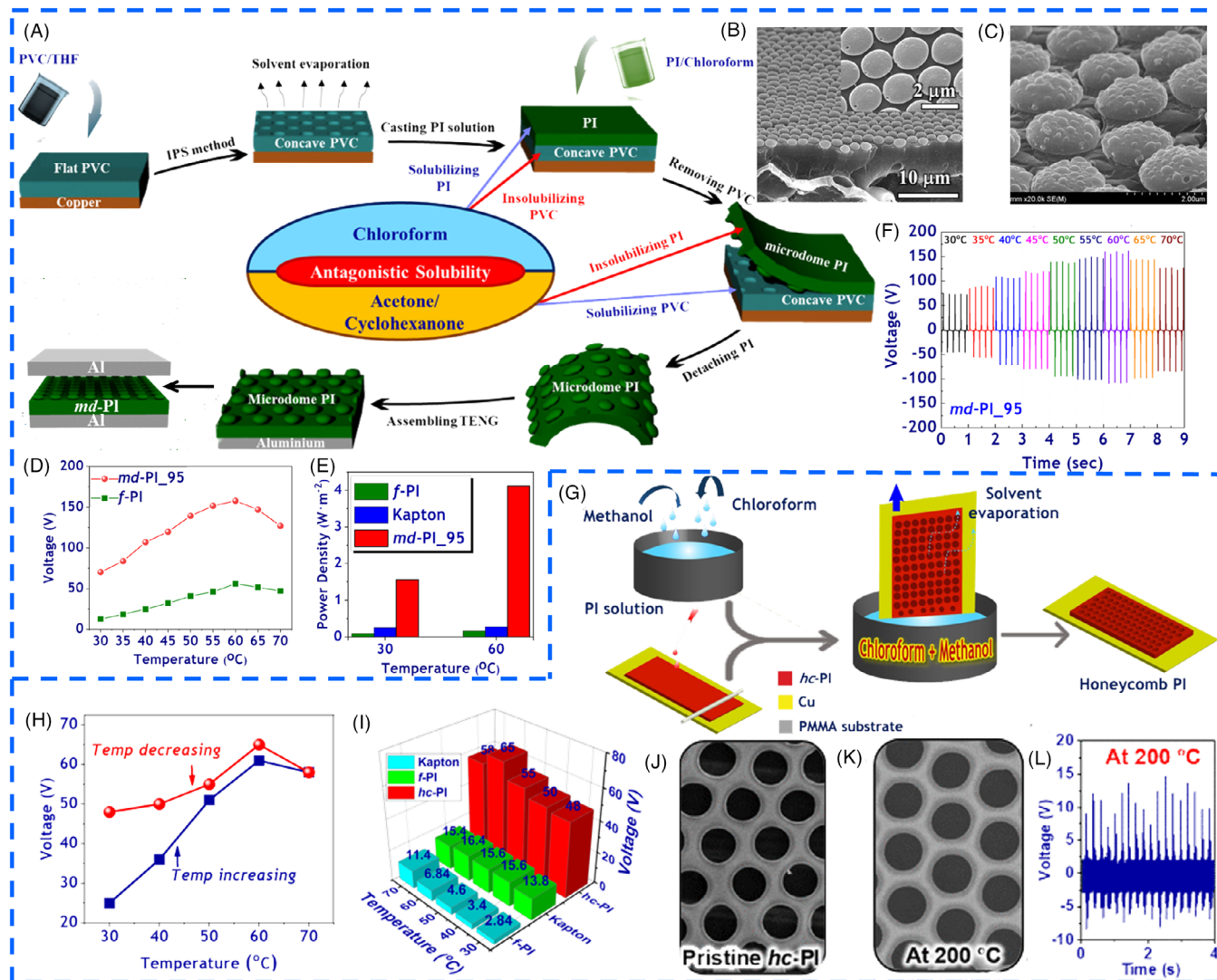


FIGURE 7 (A) Refinement of the microdome array polyimide (md-PI) film through scalable solution coating processes. (B) Cross-sectional and (C) surface views of the md-PI film. (D) Impact of temperature on V_{oc} of triboelectric nanogenerator (f-TENG) and md-PI_95-based triboelectric nanogenerator (TENG). (E) Power density of TENGs utilizing fluorinated PI (F-PI), Kapton and md-PI_95 under varying temperature conditions. (F) Voltage signals of md-PI_95 at elevated temperatures under high-temperature conditions. (G) Scheme demonstrating the fabrication of the honeycomb pattern PI (hc-PI) film employing scalable solution coating processes. (H) Impact of temperature on the output performance of hc-TENG. (I) Impact of temperature on the V_{oc} of TENGs assembled with Kapton, F-PI, and hc-PI. (J) and (K) SEM images of hc-PI before and after being thermally annealed at 200°C for 2 h. (L) Electrical output of hc-TENG at an extreme operating temperature of 200°C. *Source:* (A–F) Reproduced with permission from Ref. [106]. Copyright 2022, Elsevier. (G–L) Reproduced with permission from Ref. [105]. Copyright 2022, American Chemical Society.

TENG (md-TENG) can effectively collect windmill energy and vibration from the engine even in hot air and high humidity environments, with excellent durability of over 16 000 contact-separation cycles and better electrical outputs at elevated temperatures. As revealed in Figure 7D–F, the output voltage of the device exhibits a significant increase with rising ambient temperature, reaching a maximum value of about 158 V at 60°C. In addition, the output voltage of f-TENG (flat PI-based TENG) is much lower than that of md-TENG at each temperature point due to

a significantly smaller surface area before tribo-surface patterning. Notably, the power density of commercial Kapton, f-PI (flat PI), and md-PI_95 (the md-PI prepared with THF/MeOH of 95/5) also increases with temperature, consistent with previous studies.^{4,27,31,43} However, there is an optimal temperature point for obtaining the highest output due to the electron-driving-related factors and material-related factors.^{42,43,107} The study identifies 60°C as the ideal operating temperature for obtaining the optimal electrical output.

In sequence, Bui et al. proposed a triboelectric that can mitigate the typical defects of TENGs by utilizing a surface-patterned high-temperature-resistant thermoplastic.¹⁰⁵ Specifically, the customizable honeycomb-patterned PI (hc-PI, Figure 7G) was fabricated through a simple and scalable IPS method. The excellent heat-resistant flexible thermoplastic property of PI, along with the dead-end pore honeycomb pattern array, optimized the electrification efficiency of hc-TENG (hc-PI-based TENG, Figure 7H,I). The fabricated hc-TENG demonstrated an exceptional output power of 1.05 W m^{-2} , which is 22 times higher than the TENG assembled with normal flat PI. Notably, hc-PI could withstand temperatures up to 200°C without causing damage to the hexagonal honeycomb hole arrays while maintaining high uniformity (Figure 7J,K). As a result of this dimensional and structural stability, hc-TENG can operate stably at 200°C (Figure 7L), implying that it can be used at extreme temperatures up to 200°C or even higher. The above results demonstrate that the optimization of surface physical structures in PTMs serves as an effective strategy for enhancing their triboelectric output in high-temperature environments.

3.2.3 | Polymer composite tribo-materials

Synthetic polymer composite tribo-materials

Theoretical research on TENG devices reveals that tribo-materials not only serve as friction materials but also as storage mediums for friction charges.^{108–110} As such, the output performance of TENG devices is heavily reliant on the properties of the utilized tribo-materials. To achieve more specific and superior properties, researchers have developed triboelectric composites by doping and combining other component characteristics with those of the original tribo-materials.^{111–113} Remarkably, this strategy has demonstrated its value in producing high-output performance TENG devices. For instance, Cheng et al. created an efficient ionic liquid (IL) elastomer-based TENG (ILC-TENG, Figure 8A,B) that is flexible, stretchable, self-healing, environmentally stable, and durable by utilizing carbon nanotubes (CNTs)-doped ILC as the conductive electrode and electrospun PVDF/polyurethane (PVDF/PU) nanofibrous membrane as the tribo-layer.¹¹⁴ The PVDF/PU was autonomously adhered onto the surface of ILC electrode. After storing the assembled ILC-TENG device at -20 , 30 , and 80°C for 12 h, respectively, the relevant triboelectric output performance test results (Figure 8C) demonstrated V_{oc} values of 177.44, 182.90, and 179.18 V at each temperature point respectively, indicating excellent environmental thermal stability of the device.

As previously mentioned, polymers are currently the primary alternatives utilized in various TENG applica-

tions due to their inherent advantages such as flexibility, lightweight, and ease of large-scale preparation.^{83,84,117} However, the use of most polymer alternatives is limited by their flammability and melt-dripping issues, which can result in not only shutdown of electronic equipment but also dangerous fires. Therefore, it is crucial to develop flame-retardant tribo-materials, particularly in aerospace, transportation, fire protection, and other demanding applications. To address this issue, Chen et al. proposed a facile, robust, and cost-effective solution-casting method for preparing flame-retardant triboelectric polymer based on PVA doped with PPA-PEI polyelectrolyte (Figure 8D).¹¹⁵ The PVA/PPA-PEI film, containing 10 wt.% PPA-PEI, not only self-extinguished immediately after the burner was moved away but also improved its triboelectric properties (Figure 8F–H). Furthermore, PVA/10 wt.% PPA-PEI-based TENG (Figure 8E) could still maintain stable electrical output within a wide temperature range ($\leq 70^\circ\text{C}$), making it suitable for harsh environments. This study proposes a feasible approach to enhance the electrical and flame-retardant properties of conventional TENGs (c-TENGs), as well as broaden their application in harsh environments through the incorporation of appropriate polyelectrolytes as flame-retardant additives. Similarly, Luo et al. reported a robust and flame-retardant wood-based TENG (FW-TENG), which was prepared using a three-step process involving delignification, infiltration with bentonite nanosheets, and hot-pressing, for self-powered building fire protection.¹⁸ The FW-TENG demonstrated consistent electrical output from room temperature to 150°C , indicating its exceptional heat resistance.

Due to the susceptibility of TENG devices to high ambient temperature,^{118,119} researchers are compelled to develop a new type of TENG with stable electrical performance. Thereinto, Chen et al. crafted an AFE-based TENG (AFE-TENG) with energy harvesting, protection, and fire alarm capabilities by integrating 6AFE-25 (containing 25% urea) and 1AFE-25 (containing 25% urea).¹¹⁶ Additionally, the incorporation of CNTs and urea into 6AFE-25 has resulted in exceptional flame retardancy (Figure 8I). Figure 8J illustrates the temperature-dependent triboelectric effect of AFE-TENG within a range of 25 – 250°C . The enhanced electron transfer rate resulting from elevated temperatures leads to an increase in output voltage from the initial value of 22.70 – 28.13 V ,³¹ thereby enabling it to function as a wearable power source to activate electronics. Additionally, the AFE-TENG could also serve as a self-powered sensor to generate output electrical signals during collisions (Figure 8K,L). From Figure 8K, it can be observed that the peak voltage of AFE-TENG increased from 10.42 to 13.33 V as the temperature rose from 25 to 250°C and when the descent height reached 50 cm , indicating a positive correlation between electrical output

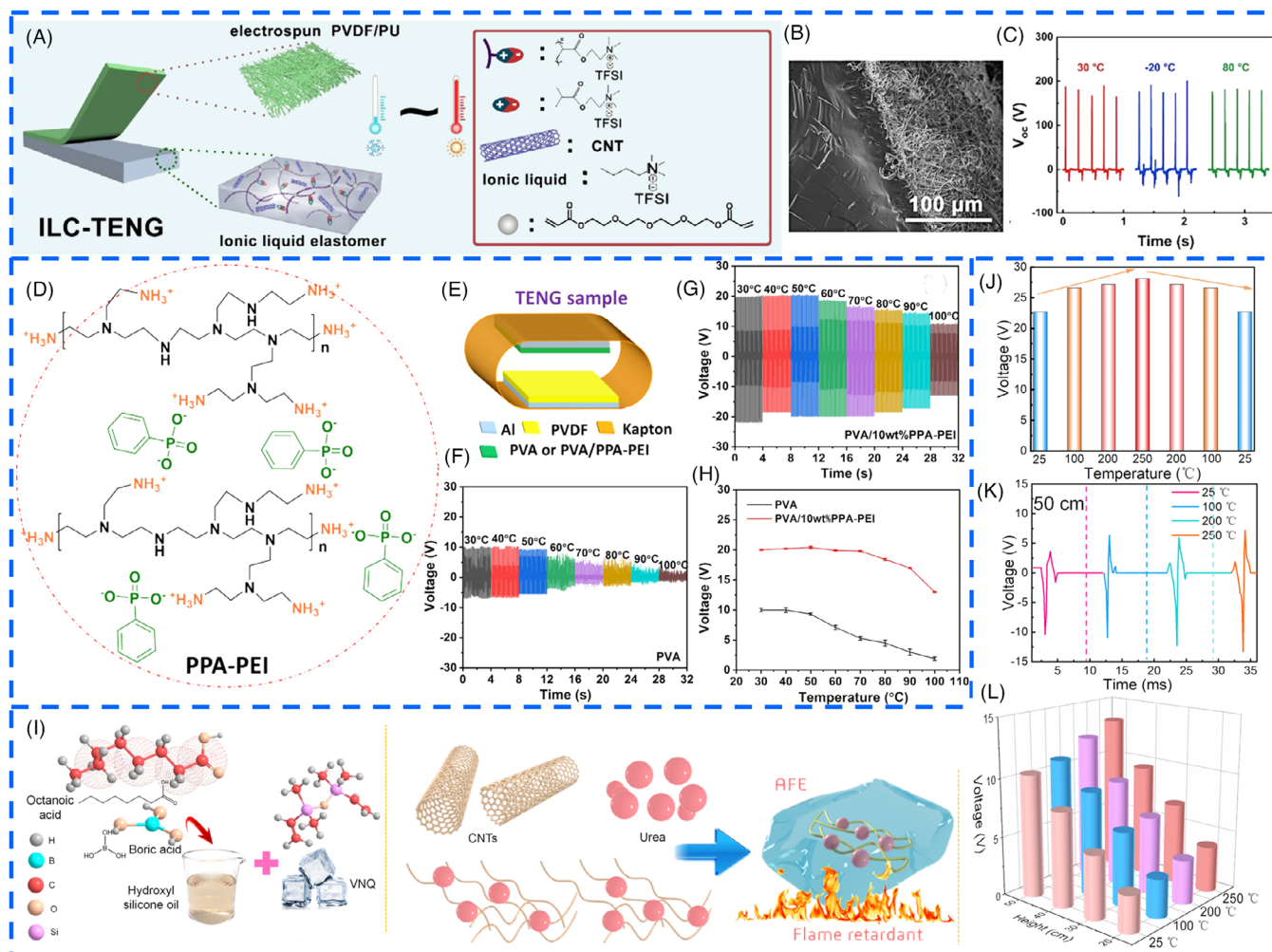


FIGURE 8 (A) Schematic diagram depicting the structural composition of ionic liquid elastomer (ILE)-triboelectric nanogenerator (TENG). (B) Cross-sectional SEM image of the ILC-TENG. (C) Comparative analysis of energy harvesting performance of ILC-TENG at varying temperatures. (D) Chemical structure of phenyl phosphonic acid-branched polyethyleneimine (PPA-PEI) polyelectrolyte. (E) Outline of the TENG's structure and materials. In-operando V_{oc} of (F) pure polyvinyl alcohol (PVA)-based TENG and (G) PVA/10 wt.% PPA-PEI-based TENG triggered by DMA with rising temperature. (H) Comparison of the V_{oc} between the pure PVA-based TENG and PVA/10 wt.% PPA-PEI-based TENG during a heating process. (I) Schematic diagram illustrating the fabrication process of the anti-impact and flame retardant elastomers (AFEs). (J) V_{oc} values of the TENG at varying temperatures. (K) The correlation of electrical output of TENG with temperature subjected to an impact force of 50 cm drop hammer. (L) 3D bar graph depicting the relationship between voltage, temperature and falling height. *Source:* (A–C) Reproduced with permission from Ref. [114]. Copyright 2022, Elsevier. (D–H) Reproduced with permission from Ref. [115]. Copyright 2020, Elsevier. (I–L) Reproduced with permission from Ref. [116]. Copyright 2022, Elsevier.

and temperature. Furthermore, Figure 8L demonstrates the voltage and temperature-dependent electric properties of AFE-TENG, providing further evidence that the device maintains stable mechanical–electrical–thermal coupling performance under various extreme conditions. Besides, Wen et al. employed micro-nanocomposites to construct a robust freestanding and single-electrode mode harsh-environmental TENG (heTENG) with wear resistance, high-temperature endurance, and high hardness, enabling it to efficiently collect sliding/vibration energy and self-powered vibration sensing.⁶⁶ Remarkably, the heTENG device can operate within a wide temperature range of –30

to 550°C. However, the impact of temperature on the output performance of heTENG was not investigated in this particular study.

Moreover, our group has conducted relevant and significant research in this field.^{120,121} Our efforts culminated in the design of a groundbreaking thermo-regulating TENG (Tr-TENG) that leverages phase change materials (PCMs) to mitigate the thermal negative impact of PTMs and maintain high-temperature steady electrical performance, as depicted in Figure 9A,B.¹²⁰ The Tr-TENG is composed of a sheath/core electro-spun fiber membrane and conductive elastic fabric, enabling the simultaneous harvesting of

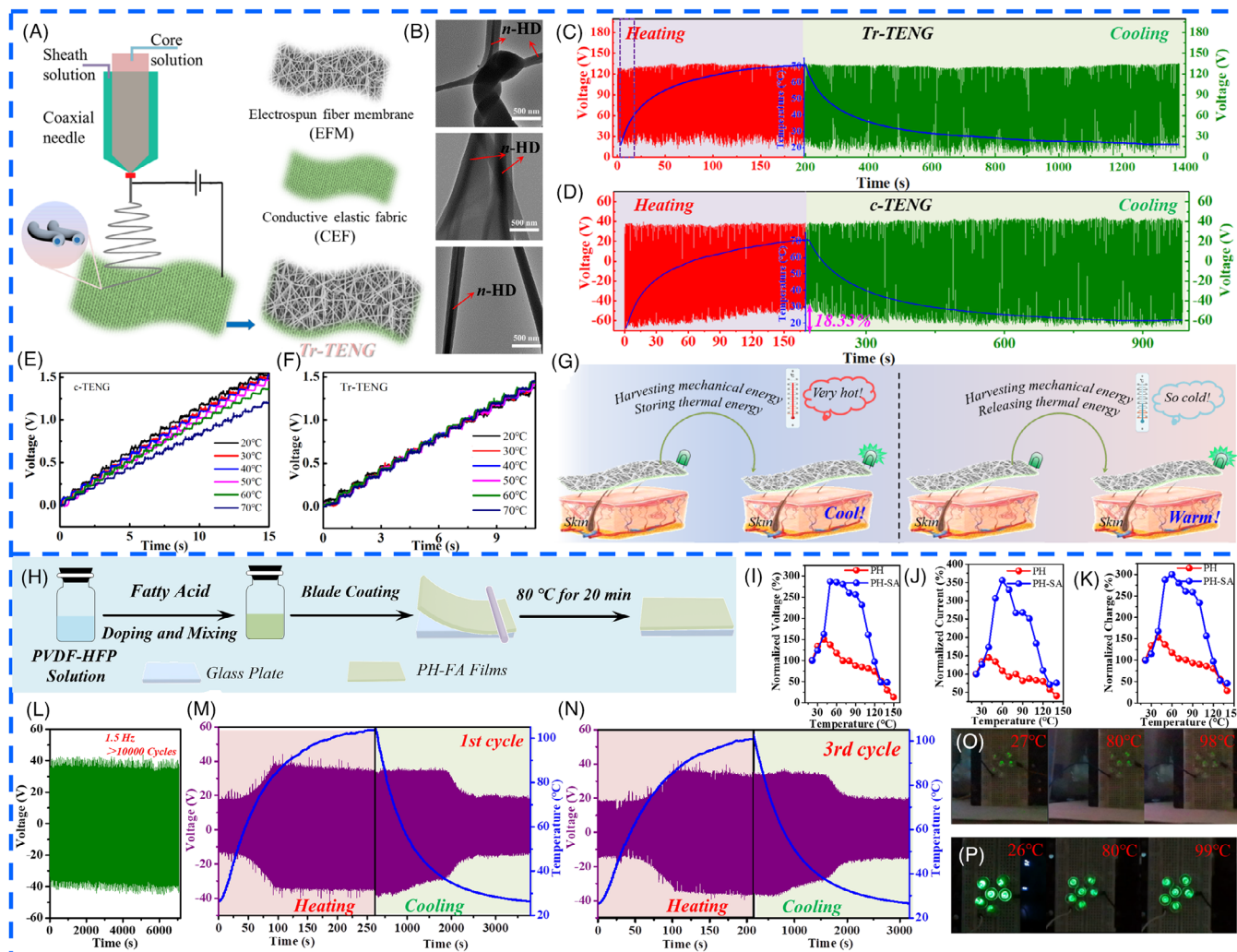


FIGURE 9 (A) Flowchart depicting the process of fabricating a thermo-regulating triboelectric nanogenerator (Tr-TENG) through coaxial electro-spinning technique. (B) TEM micrographs of the EFM3 electro-spun fiber membrane with a sheath/core structure. (C) V_{oc} of the Tr-TENG based on EFM3 during the heating and cooling (the temperature range of Tr-TENG in the purple dotted box was 20–40°C, which corresponds to the melting-phase-transition process of *n*-HD). (D) V_{oc} of the control TENG (conventional TENG [c-TENG]) based on pure electro-spun poly(vinylidene fluoride-co-hexafluoropropylene) (polyvinylidene fluoride [PVDF]-HFP) fiber membrane (c-EFM) during heating and cooling. Charging performance of (E) the Tr-TENG and (F) c-TENG as a capacitor (50 V, 0.47 μ F) at different temperatures. (G) Schematic diagram of Tr-TENG for application in wearable smart electronic devices. (H) Fabrication process for fatty acid-doped PVDF-HFP films (PH-FA). Normalized voltage (I), current (J), and charge (K) of pure PVDF-HFP (PH) and stearic acid-doped PVDF-HFP (PH-SA) films. (L) Stability and robustness evaluation of PH-SA-based TENG at 100°C. (M and N) V_{oc} of PH-SA-based TENG during continuous heating and cooling. Photos of (O) PH and (P) PH-SA-based TENGs to light up six LEDs at varying temperatures. *Source:* (A–G) Reproduced with permission from Ref. [120]. Copyright 2021, American Chemical Society. (H–P) Reproduced with permission from Ref. [121]. Copyright 2023, Elsevier.

both mechanical and thermal energy. By integrating PCMs and triboelectric materials, as illustrated in Figure 9G, the wasted mechanical and heat energy generated by friction and thermal stresses in the environment could be effectively recycled and utilized. Results from Figure 9C,D clearly indicate that the Tr-TENG could uphold a steady output performance without any deterioration resulting from the introduction of PCMs, even during continuous heating and natural cooling, whereas the output perfor-

mance of c-TENG deteriorated by 18.33%. Figure 9E,F presents the charging performance of the c-TENG and Tr-TENG, which once again confirms that the fabricated Tr-TENG is capable of maintaining a stable electrical output within a wide temperature range, effectively suppressing the negative effect of the heat energy generated by friction and the environmental thermal energy on the output performance of the TENG. More importantly, the Tr-TENG exhibits high-efficiency thermal management

ability, as shown in Figure 9F, resulting in improved durability, reliability, and thermal comfort.

Additionally, recent studies have revealed that the incorporation of appropriate liquid lubrication not only confers superlative wear resistance to TENGs by inhibiting the wear and transfer of PTMs but also enhances their electrical outputs.^{83,122–125} In light of this, our group employed blade coating technology to fabricate a series of fatty acid (FA)-doped PVDF-HFP (PH-FA) PTM films with optimized ratios, as depicted in Figure 9H.¹²¹ Here, the FA was utilized to enhance the electronegativity of PVDF-HFP PTM and simultaneously employed as lubrication additive to improve the wear resistance. As shown in Figure 9I–K, the PH-SA PTM exhibited exceptional electrical output characteristics with V_T/V_{Room} , I_T/I_{Room} , and Q_T/Q_{Room} (output efficiency) values at 100°C reaching unprecedented levels of 231.10%, 251.46%, and 234.01% respectively, which have not been reported in previous studies related to PTM-TENG.^{4,25,42–44,120,121,126,127} Furthermore, the PH-SA-based TENG exhibits exceptional stability, durability, and repeatability as evidenced by its consistent output performance during continuous heating and cooling thermal cycles, even after three such cycles, and in high-temperature environments up to 100°C (Figure 9L–N). Moreover, in comparison to PH, the PH-SA-based TENG could still illuminate six LEDs in a high-temperature operating environment of approximately 100°C, with no significant change in brightness (Figure 9O,P). Our research not only opens up new possibilities for developing advanced multifunctional TENGs with desirable characteristics but also greatly promotes the application of TENG electronic devices in harsh or extreme temperature environments.

Natural polymer composite tribo-materials

Most synthetic polymer materials are associated with complex fabrication processes. While their widespread use in energy engineering,^{128–130} these materials present a challenge to environmental sustainability due to their origin from nonrenewable and hard-to-degrade petrochemicals in the natural environment.^{131,132} Conversely, biomass-derived natural polymer materials offer an inexhaustible and sustainable resource, presenting significant advantages in the exploitation of high-performance materials due to their unique hierarchical and porous structure.^{133–134} Therefore, these natural polymer materials present an appealing alternative to synthetic materials, as they offer a more environmentally friendly and sustainable option for the development of advanced materials.^{135–137}

Cellulose, which is widely found in green plants and other biomass, is an abundant and sustainable natural polymer material with a unique multidimensional structure, controllable surface chemistry, and excellent

thermal and chemical properties.^{138–140} It can exhibit particular tolerability, compared to other dielectric materials, by reasonable physical and chemical regulation while maintaining remarkable stability performance even under extreme environmental conditions such as high temperature and humidity.^{139,141} Therefore, the multi-scale engineering optimization and further development of cellulosic triboelectric materials with a wide range of temperature resistance can pave the way for superior feasibility in applying TENGs under adverse temperature environmental conditions.

Recently, Luo et al. developed a wood-based TENG using natural linden wood that underwent chemical pretreatment and hot-pressing to remove lignin and hemicellulose while retaining cellulose in a simple and effective three-step strategy (Figure 10A,B). The as-synthesized TENG maintained 60.5% of its original power output even at high temperatures of up to 250°C, as depicted in Figure 10C.¹⁸ In a similar vein, Wang et al. created a flame-retardant cellulose-based TENG (FR-TENG) by incorporating BP and PA as flame retardants, as illustrated in Figure 10D.¹⁴² The CNF-BP-PA/AgNWs composite film exhibited a layered structure of tannic acid-modified black phosphorus nanosheet that acted as a physical barrier (Figure 10E), whereas PA facilitated dehydration and coking of the composite material, thereby synergistically achieving excellent fire resistance and flame retardancy, resulting in a stable electric output performance of FR-TENG, as demonstrated in Figure 10F,G.

In addition, as described in Figure 11A, Gao et al. utilized a combination of casting and hot-pressing strategy to fabricate a novel chitosan/di-aldehyde nanocrystalline cellulose (DANC)-based triboelectric material (CDTM) that was used for energy harvesting in severe atmospheric conditions.¹²⁹ The stable Schiff base structure (Figure 11B) formed between the amino group of chitosan and the aldehyde group of DANC enhanced the internal binding of CDTM, ensuring its stability under harsh conditions.¹⁴³ Meanwhile, the active amino group of chitosan improved the electron-donating ability of the CDTM,¹⁴⁴ thereby improving the triboelectric output performance of CD-TENG (Figure 11C,D). Importantly, the CD-TENG demonstrated resistance to various environmental factors such as temperature, humidity, and UV radiation (Figure 11E). Experimental results (Figure 11F) showed that the V_{oc} change rate of the constructed CD-TENG was significantly lower than that of a regular paper matrix at 99 RH% and only 2% at 100°C, demonstrating excellent environmental interference resistance. Zhao et al. presented a three-step strategy (mild hydrolysis, freeze-drying, and in situ growing, Figure 11G) for large-scale production of bamboo/polyaniline triboelectric material (BPTM) with unique nanostructures.¹³⁰ Figure 11H,I illustrates the

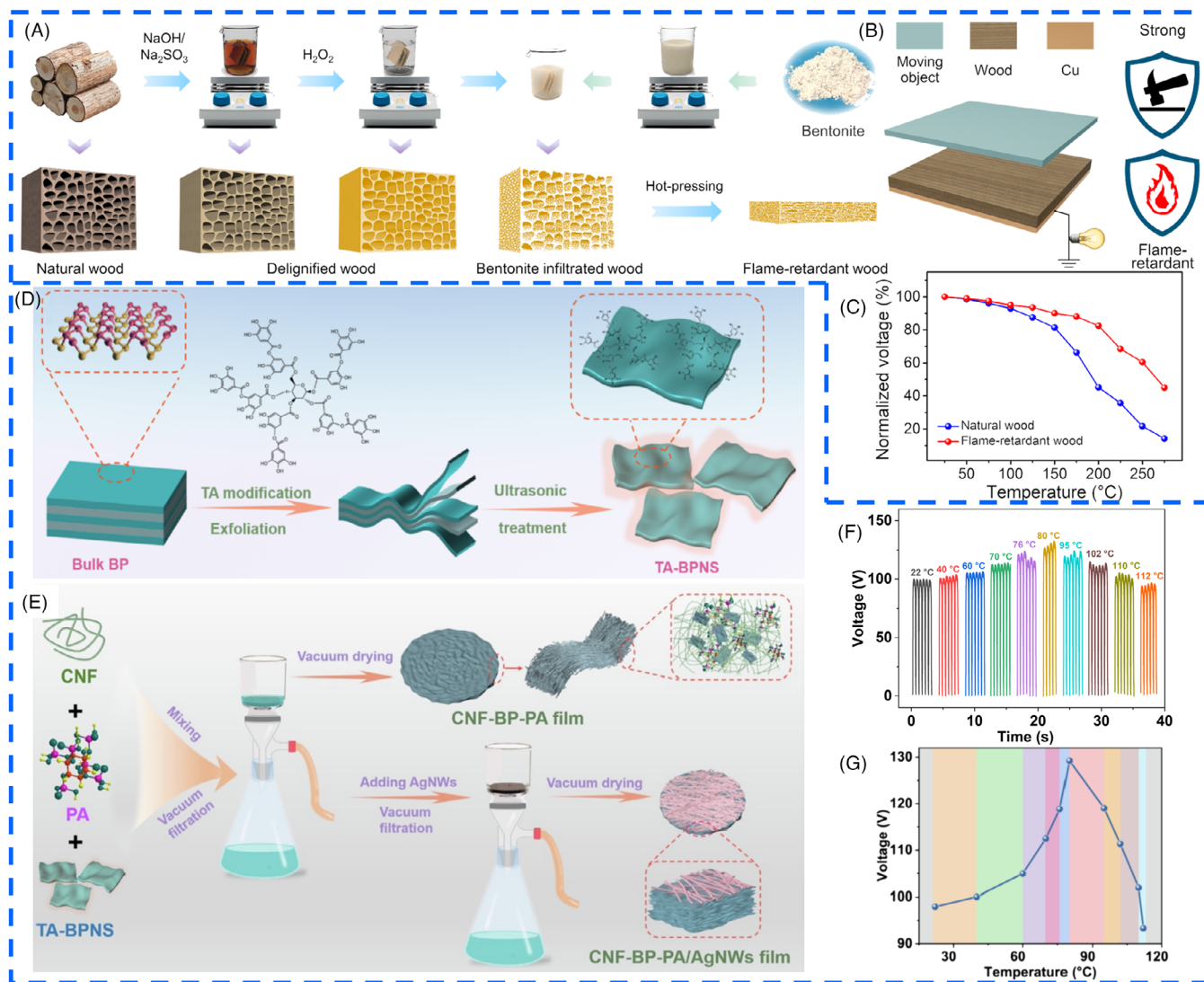


FIGURE 10 (A) Process flow diagram for the production of fire retardant wood. (B) Structural diagram of flame-retardant wood-based triboelectric nanogenerator (TENG) (FW-TENG). (C) Normalized voltage of the FW-TENG and natural wood-based TENG at different temperatures. (D) Schematic diagram of tannic acid-modified black phosphorus nanosheets (TA-BPNS). (E) Preparation process for fabricating TA-BPNS, phytic acid (PA)-doped cellulose nanofibers (CNF) (CNF-BP-PA) film, and CNF-BP-PA/AgNWs film. V_{oc} (F) and V_{oc} -temperature relationship curve (G) of CNF-BP-PA/AgNWs composite film at various temperatures. *Source:* (A–C) Reproduced with permission from Ref. [18]. Copyright 2022, Elsevier. (D–G) Reproduced with permission from Ref. [142]. Copyright 2022, Elsevier.

hierarchical porous structure of BPTM and the underlying working mechanism of BPTM-based TENG, respectively. Due to the unique hierarchical porous structure of the fabricated BPTM, the BPTM-based TENG retained 85% of its triboelectric output characteristic even under extreme temperatures (200 and -196°C) and continuous thermal impacts ($\Delta T = 396^{\circ}\text{C}$), as demonstrated in Figure 11J–M. These studies significantly expand the application scope of cellulosic triboelectric material-based TENGs, offering novel insights for developing next-generation self-powered smart devices that can operate in extreme temperature environments.

3.3 | PTMs-based HTO-TENG with enhanced electrical output

The mechanisms of triboelectrification in polymers have been the subject of intense debate in recent years due to their critical role in mechanical energy harvesting by TENG devices,¹⁴⁵ prevention of electric discharge from accumulated surface charge and protection of electric devices,¹⁴⁶ as well as enhancement of particle separation in filters.¹⁴⁷ The focus of this debate has centered on electron transfer and covalent bond breaking as potential dominant mechanisms for polymer triboelectrification. The latter

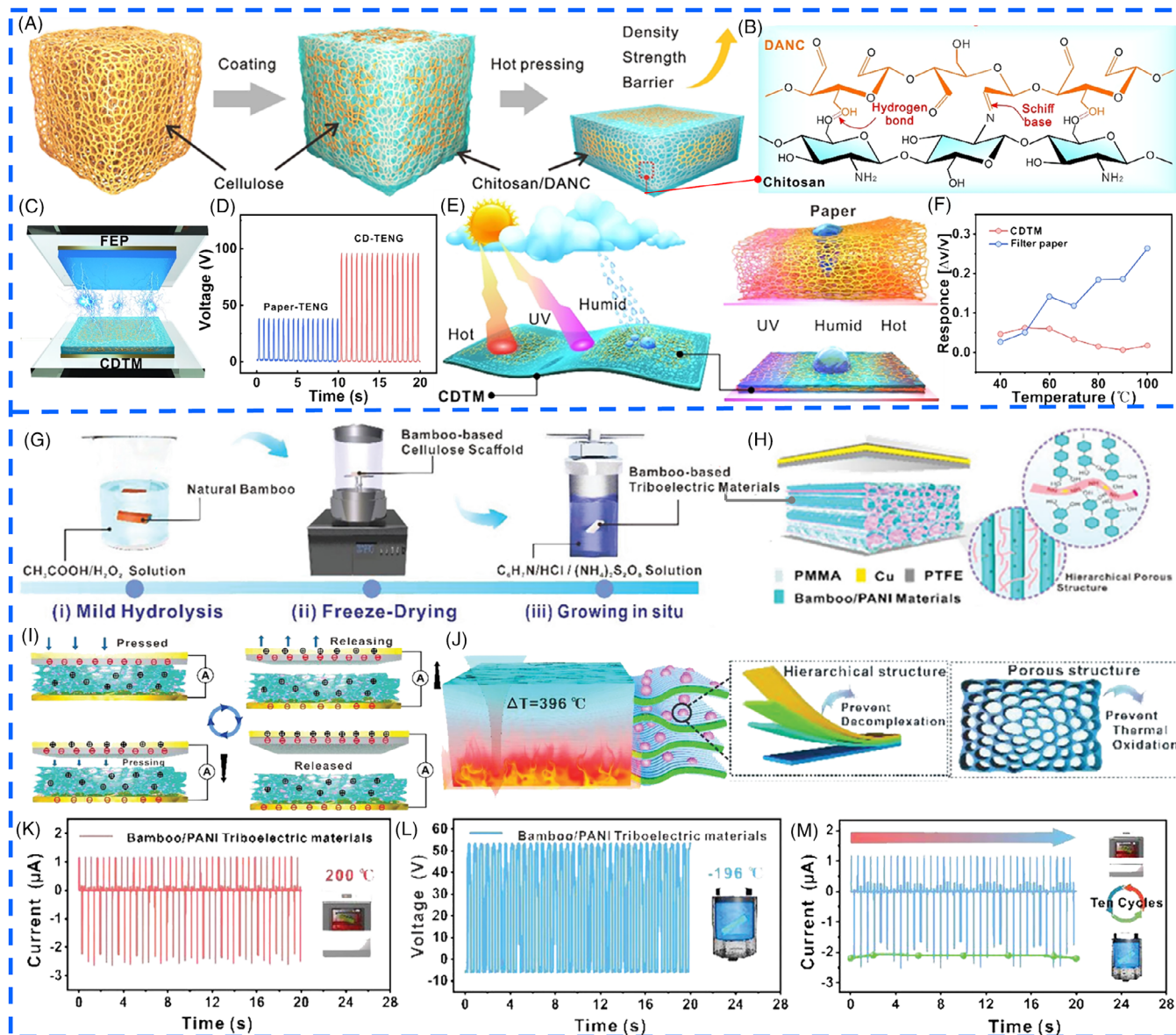


FIGURE 11 (A) Schematic diagram illustrating the morphological transformation process during the preparation of chitosan/di-aldehyde nanocrystalline cellulose (DANC) bio-based triboelectric materials (CDTM). (B) The interface binding effect between chitosan and DANC. (C) Structural diagram of CDTM-based triboelectric nanogenerators (TENGs) (CD-TENG). (D) Comparison of the V_{oc} between cellulose paper-based TENG and CD-TENG. (E) Structure diagram of cellulose paper and CDTM. (F) Changes in electrical output stability of CD-TENG across a temperature range of 30–100°C. (G) Flowchart of the primary reaction process for fabricating bamboo/polyaniline (PANI) triboelectric materials (BPTM). (H) Structural diagram of BPTM-based TENG and the hierarchical porous architecture of BPTM. (I) Operating mechanism of BPTM-based TENG. (J) Sketch diagram depicting the mechanism of hierarchical porous BPTM resistant to extreme environments. V_{oc} (K) and I_{sc} (L) of BPTM-based TENG after undergoing thermal treatment at 200°C and low-temperature treatment at -196°C, respectively. (M) I_{sc} of BPTM-based TENG after 10 impacts at temperatures ranging from -196 to 200°C. Source: (A–F) Reproduced with permission from Ref. [129]. Copyright 2023, Elsevier. (G–M) Reproduced with permission from Ref. [130]. Copyright 2022, Wiley-VCH.

mechanisms, heterolytic covalent bond cleavage (heterolysis or heterolytic fission) has been gaining recognition as a credible mechanism for polymer triboelectrification. In fact, Šutka et al. demonstrated for the first time that the dramatic increase in triboelectrification of glassy polymers upon transitioning to a rubbery state,¹⁴⁵ as well as

CE, can be modulated by intramolecular forces within the polymer bulk and adhesive forces at the contact interface. This confirms the breakage of covalent bond as a mechanism for triboelectrification in polymer insulators, without requiring chemical interaction between different polymers.¹⁴⁸ As presented in Figure 12A,B, the net

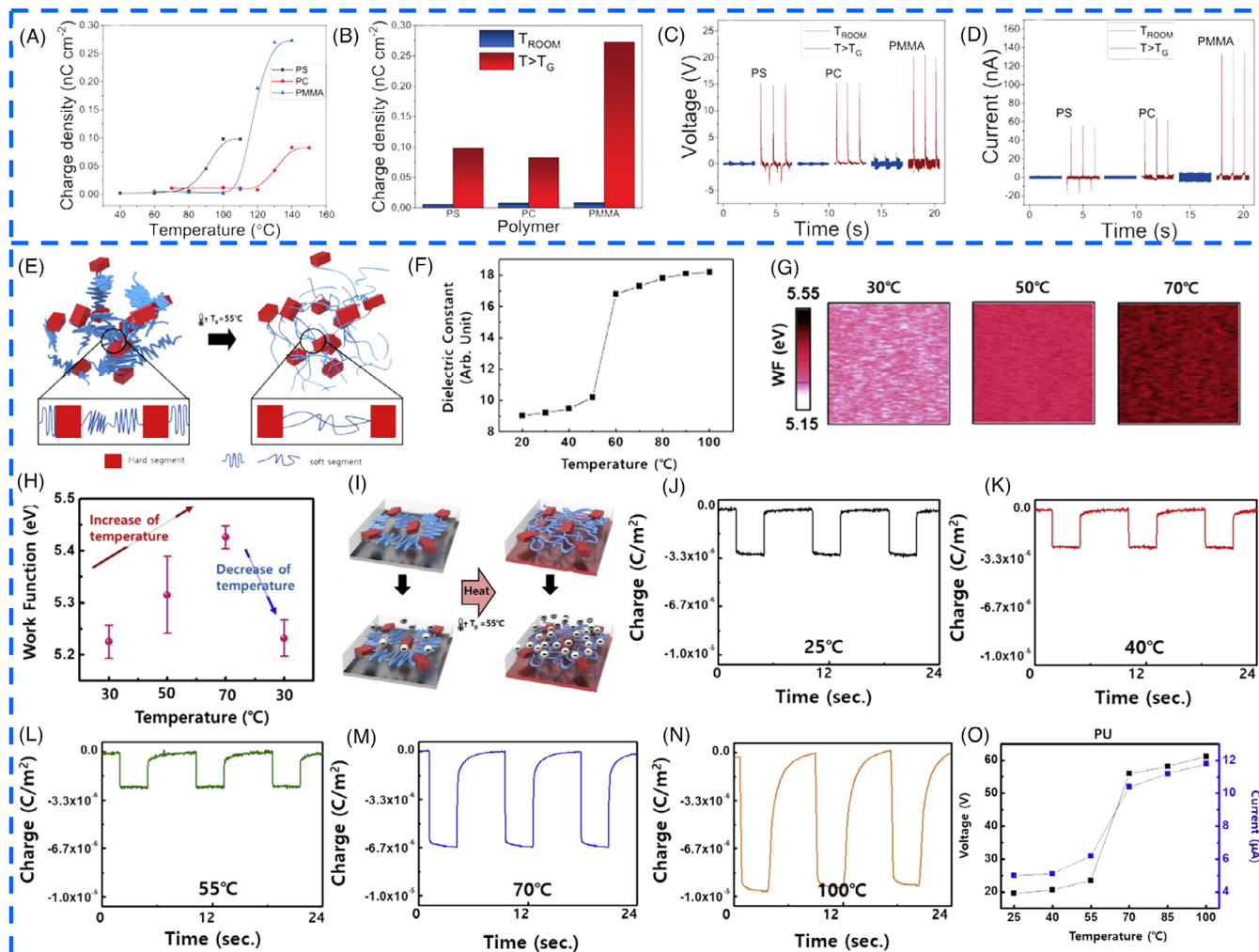


FIGURE 12 (A) Charge density shows a sharp rise as the temperature of the triboelectric nanogenerator (TENG) device reaches the corresponding glass transition temperature (T_g) of the polymer. (B) Charge density at a temperature above T_g differs by an order of magnitude from that at room temperature. (C) V_{oc} and (D) I_{sc} of polymers at room temperature and temperatures above T_g . (E) Schematic illustrations of polyurethane (PU) below and above its T_g of 55°C, respectively, depict the PU structure consisting of a hard segment and two types of soft segments. (F) Temperature-dependent variation in the dielectric constant of PU. (G) Temperature-dependent maps of the work function for PU and (H) its corresponding work function change. (I) Illustration of charge transfer mechanism pre- and post-surface rubbing of PU at varying temperatures. (J)–(N) Temperature-dependent transferred charge density of PU. (O) Temperature-dependent variations in the triboelectric voltage and current of PU. *Source:* (A–D) Reproduced with permission from Ref. [145]. Copyright 2020, The Royal Society of Chemistry. (E–O) Reproduced with permission from Ref. [149]. Copyright 2020, Elsevier.

surface charge for all studied polymers exhibited a significant increase by more than one order of magnitude when the temperature reaches the glass transition point. For instance, the surface charge of polycarbonate only increased from 0.006 to 0.011 nC cm⁻² as the temperature rises from room temperature to 110°C. Notably, the qualitative measures of electrical output for TENG devices, such as V_{oc} and I_{sc} , are also increased, as demonstrated in Figure 12C,D. This research provides theoretical guidance for the construction of TENG devices that can efficiently collect high-temperature mechanical energy.

Meanwhile, recent studies on PU, a glassy polymer, as a triboelectric material have confirmed the aforementioned

conclusion: When the temperature exceeds the glass transition temperature (T_g) of the glassy polymer, there is a significant increase in electrical output for the relevant TENG devices.¹⁴⁹ Sohn et al. introduced a glassy polymer-based PU as a tribo-layer to improve output performance of TENG and proposed a new method for making TENG devices operate stably and efficiently at elevated temperatures through friction.¹⁴⁹ Figure 12E illustrates the PU structure consisting of hard and soft segments, with the soft segment typically being a polyether block that can be formed a reversible phase due to molecular motion.^{150,151} Above T_g , PU undergoes a glass transition from a glassy state to a rubbery state. From Figure 12F,H, the dielectric

constant and work function of the PU tribo-layer initially increased slightly with temperature, followed by a sudden increase near T_g , which is in contrast to the general trend of decreasing dielectric constants for conventional polymers as temperature increases. As displayed in Figure 12G,H, the work function of PU increased by 0.2 eV as sample temperature rose from 30 to 70°C. It is well known that the triboelectric output performance is directly affected by the number of transferred triboelectric charges.^{152,153} From Figure 12I–N, the transferred charge density of PU was almost constant while the sample temperature increased from 25 to 55°C, indicating that PU is in a glassy state. However, after undergoing a glass transition, the transferred charge density drastically increased, indicating the rubbery state. Therefore, PU in rubbery state can store more charges than in glassy state, leading to enhanced output performance of TENG (Figure 12O) due to higher dielectric constant, work function, and trap sites. This finding not only suggests an intriguing approach to increase the output performance of TENG by reusing abandoned heat energy but also offers a new perspective on selecting appropriate polymers as a triboelectric layer.

3.4 | Other PTMs-based HTO-TENG

In Figure 13A, Graham et al. demonstrated the utilization of plastics extracted from the waste stream and electronic waste commonly found in households to fabricate a smart-home-applicable TENG (SHA-TENG) capable of harvesting mechanical energy generated by everyday human activities.¹⁵⁴ The electrical output was measured after 15-min intervals while incubating the SHA-TENG under varying temperature conditions. V_{oc} measurements were taken at regular intervals, as shown in Figure 13B,C. The results indicated that the output performance of the SHA-TENG remained stable even when subjected to harsh environmental conditions, highlighting its potential as a lightweight and durable device for smart homes. Similarly, to address the issues of waste pollution and efficient energy generation, Chougale et al. proposed a unique approach utilizing discarded soda cans and plastic cups through a simple function change (Funchange) TENG, which offers the added benefit of avoiding chemical processing (Figure 13D).³⁰ As displayed in Figure 13E, the Funchange TENG device exhibited exceptional output performance. The effect of temperature on the tribolayers of the Funchange TENG device was also tested at various temperature conditions, with results indicating minimal impact on its output performance. Such methods of utilizing waste materials in high-performance TENG devices provide a valuable reference for sustainable, convenient, clean, and environment-friendly energy collection.

Additionally, as displayed in Figure 13F–N, Rodrigues, Cheng, and Shi et al. also constructed a series of PTM-based TENG devices.^{44,45,121} The research findings indicate that these devices could effectively harvest mechanical energy at high temperatures of 70, 220, and 250°C respectively, showcasing their potential for high-temperature operation. Nevertheless, the electrical output performance of the corresponding TENG devices shows considerable attenuation under such elevated temperatures, presenting challenges for the practical applications.

3.5 | Gel-based HTO-TENG

TENG represents an emerging technology in energy harvesting, medical treatment, and information technology.¹⁵⁶ As stretchable and multifunctional electronics continue to advance, there is a growing demand for TENGs that have comparable stretchability and functionality.¹⁵⁷ Unfortunately, although there are many candidate materials for flexible tribo-layers,¹⁵⁸ options for flexible and bionic-skin electrode materials are still quite limited. Traditional flexible conductive materials like silver paste, silver nanowires, CNTs, and graphene are not ideal for mass production due to their ultrahigh cost or complicated preparation processes.^{159–161} Therefore, it is urgent to explore and develop high-performance flexible bionic-skin electrode materials for TENGs used in electronics.

3.5.1 | Hydrogels/organohydrogels-based HTO-TENG

Distinguished from conventional flexible conductive materials, hydrogels in solid form consist of hydrophilic polymer networks that are swollen with water or ionic aqueous solution and directly embed the conductive phase within the polymer micro-networks.^{157,162} This unique feature ensures the continuity of the conductive phase throughout deformation processes, resulting in exceptional electrical conductivity, stretchability, and adhesion.^{162,163} Meanwhile, the 3D network architecture of hydrogels endows them with outstanding mechanical properties,^{164,165} such as high flexibility, softness, and elasticity, rendering them an ideal material for realizing flexible and stretchable TENGs.

Various efforts have been made to design and develop flexible TENG devices capable of stable operation in extreme environments due to the remarkable properties of the aforementioned hydrogels.^{165–168} Chen et al. fabricated a thin hydrogel membrane using a solution replacement treatment method.¹⁶⁵ The double-network ionic hydrogel membrane serves as both the flexible electrode and

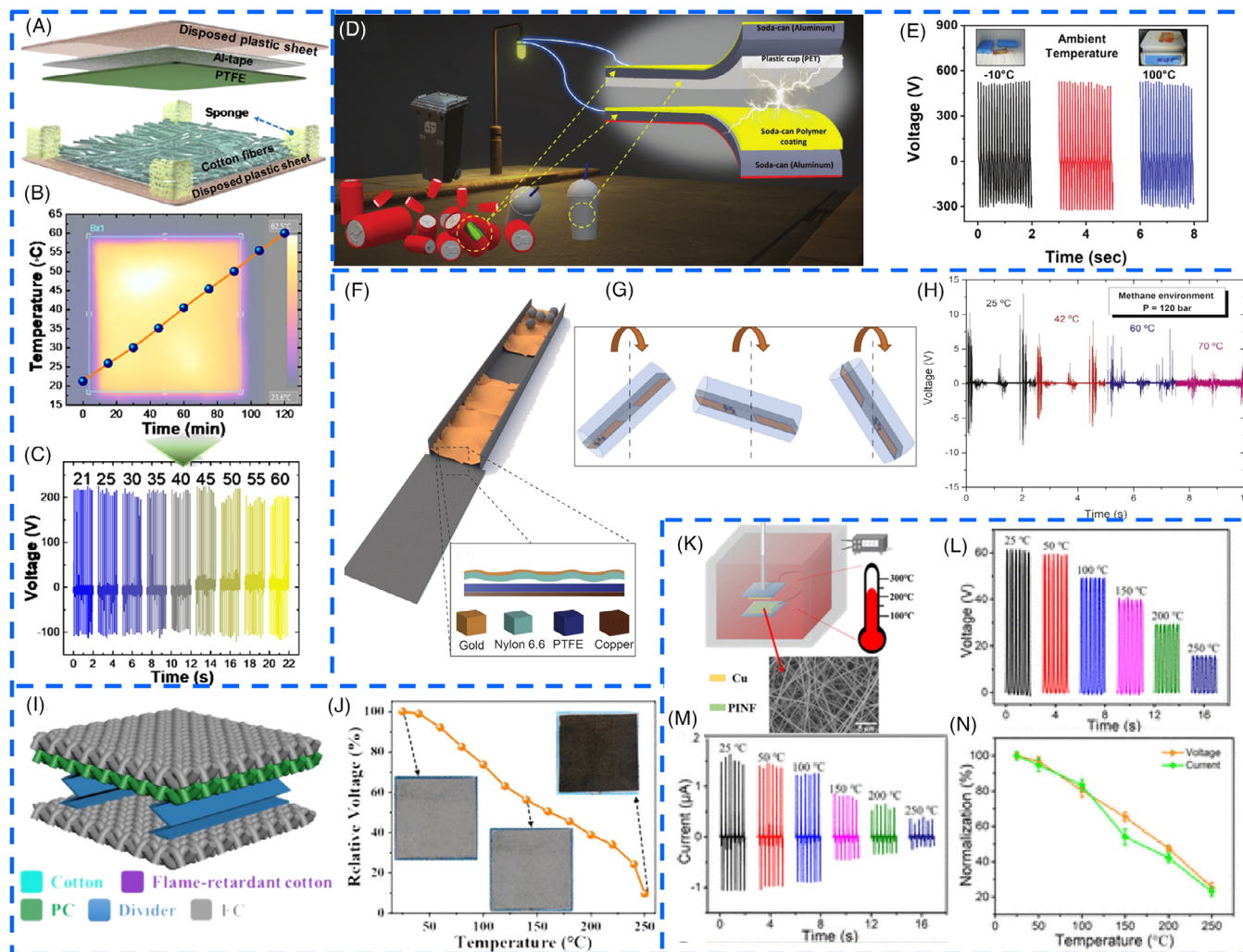


FIGURE 13 (A) Components of the smart-home-applicable (SHA)-triboelectric nanogenerator (TENG). (B) and (C) SHA-TENG durability test under different temperature conditions and measured V_{oc} curves. (D) Schematic diagram of the Funchange TENG utilizing aluminum soda cans and disposable plastic cups. (E) Output performance of Funchange TENG under varying temperature conditions. (F) Design of structural configuration for high-temperature triboelectric material testing setup. (G) Schematic depiction of the rotation movement of the assembled device. (H) Temperature-dependent variation of the V_{oc} for the assembled device under constant pressure conditions. (I) Schematic diagram of the flame-retardant textile-based TENG (FT-TENG). (J) Relative voltage of the FT-TENG at different temperatures, and the illustrations depict photographs of the device operating at 25, 140, and 250°C. (K) Schematic diagram of the polyimide nanofiber-based TENG (PINF-TENG) characterized for energy harvesting at high temperatures. (L) V_{oc} and (M) I_{sc} of the PINF-TENG under different temperatures. (N) Normalized voltage and current of PINF-TENG. *Source:* (A–C) Reproduced with permission from Ref. [154]. Copyright 2020, Elsevier. (D and E) Reproduced with permission from Ref. [30]. Copyright 2021, Wiley-VCH. (F–H) Reproduced with permission from Ref. [155]. Copyright 2020, Elsevier. (I and J) Reproduced with permission from Ref. [44]. Copyright 2020, American Chemical Society. (K–N) Reproduced with permission from Ref. [45]. Copyright 2022, American Chemical Society.

triboelectric layer in the constructed EHTS device, demonstrating excellent stretchability and a wide application temperature range (-10 to 40°C). The output signals of the EHTS are generated around a peak voltage of about 10 V without noticeable variations over a wide temperature range from -10 to 40°C . Bao et al. synthesized an anti-freezing hydrogel via one-step radical polymerization of acrylamide monomer in hydroxyethyl cellulose aqueous solution (Figure 14A),¹⁶⁶ which improved mechanical properties and provided water retention. As depicted in

Figure 14B, a single-electrode mode AH-TENG with a sandwiched structure was constructed, with the AH serving as the conductive electrode and silicone rubber thin layers employed as triboelectric layers at both top and bottom. Analysis of the electrical output of AH-TENG under different temperatures revealed that the V_{oc} and I_{sc} at -20 and 20°C exhibited only a small difference (Figure 14C). Furthermore, the AH-TENG could operate at a temperature of 60°C , but there was an obvious attenuation in electrical output at 60°C compared to

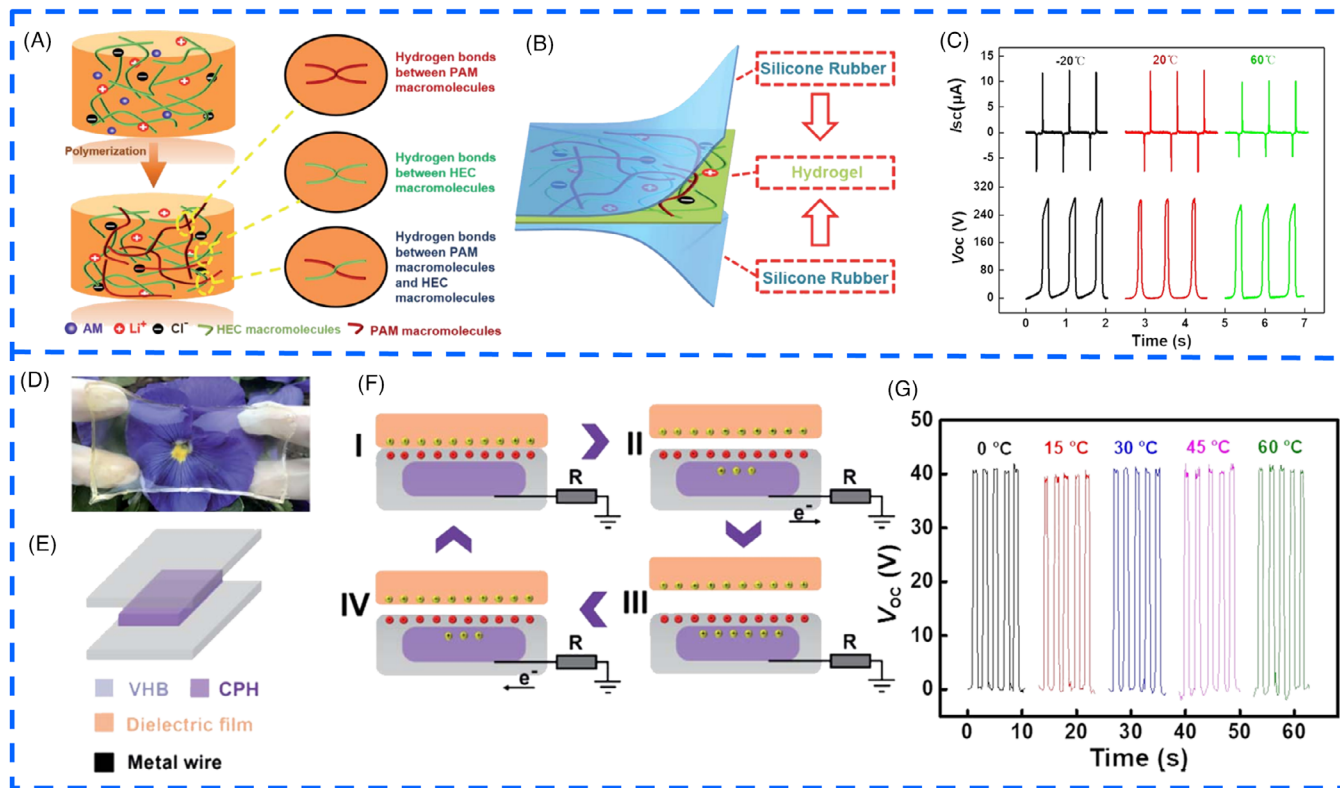


FIGURE 14 (A) Schematic diagram of the polymerization process of anti-freezing hydrogels (AH). (B) Structural diagram of the anti-freezing hydrogel-based triboelectric nanogenerator (TENG) (AH-TENG). (C) V_{oc} and I_{sc} of AH-TENG at -20 , 20 , and 60°C . (D) Photograph of cellulose/PVA hydrogel (CPH). (E) Design of CPH-TENG. (F) Schematic illustration of the working mechanism of CPH-TENG. (G) V_{oc} of CPH-TENG at five distinct temperatures. *Source:* (A–C) Reproduced with permission from Ref. [166]. Copyright 2020, The Royal Society of Chemistry. (E–G) Reproduced with permission from Ref. [167]. Copyright 2020, The Royal Society of Chemistry.

that at 20°C due to the competing effect between thermal fluctuation and mechanical properties.⁴³ Wang et al. fabricated an ionic conductive CPH through a facile and environment-friendly strategy with zero wastage, as displayed Figure 14D.¹⁶⁷ The V_{oc} value of CPH-based TENG exhibited no significant variation in the range of 0 – 60°C (Figure 14E–G), indicating that the CPH-based TENG for energy harvesting showed resistance to temperature change, further expanding the applicability of self-powered wearable electronic devices.

Hydrogels possess excellent properties such as electrical conductivity, flexibility, stretchability, and biocompatibility,^{174–175} but their mechanical properties are highly unstable due to water loss or absorption caused by environmental factors during applications.^{174,176–178} To address this issue, researchers have developed organohydrogels that replace water molecules with organic solvent molecules to enhance antifreeze and water retention capabilities.^{174–176} The resulting conductive organohydrogels, including MMCOHs (Figure 15A–C),¹⁶⁹ PAAm-Clay-KI organohydrogel (Figure 15D,E),¹⁷⁰ PAAm-clay organohydrogel (Figure 15F–I),¹⁷¹ and AVN organohydrogel (Figure 15J,K),¹⁷² displayed superior temperature resistance and stretchability, making them

ideal electrodes for TENG devices. These devices maintain stable electrical output performance in a range of temperatures (-60 to 60 , -20 to 80 , -30 to 80 , and -50 to 100°C) due to the HTO characteristics of the organohydrogels. Furthermore, Khan et al. created fully self-healing TENG devices utilizing highly stretchable and anti-freezing conductive self-healable organohydrogels (CSOs) as electrode and nonconductive self-healable organohydrogels (NSOs) as triboelectric materials. As-fabricated CSO-TENG displayed increasing electrical outputs with rising temperature (Figure 15L),¹⁷³ which can be attributed to the increased conductivity resulting from the free movement of ions within the conductive organohydrogel at elevated temperatures (Figure 15M). Conversely, lower outputs were observed at subzero temperatures due to the ice coating formed on the surface of the tribo-layer reducing the active area.

3.5.2 | Ionogels/ionic elastomer-based HTO-TENG

Ionogels, which are polymer networks saturated with ILs,^{178,179} have garnered significant interest from

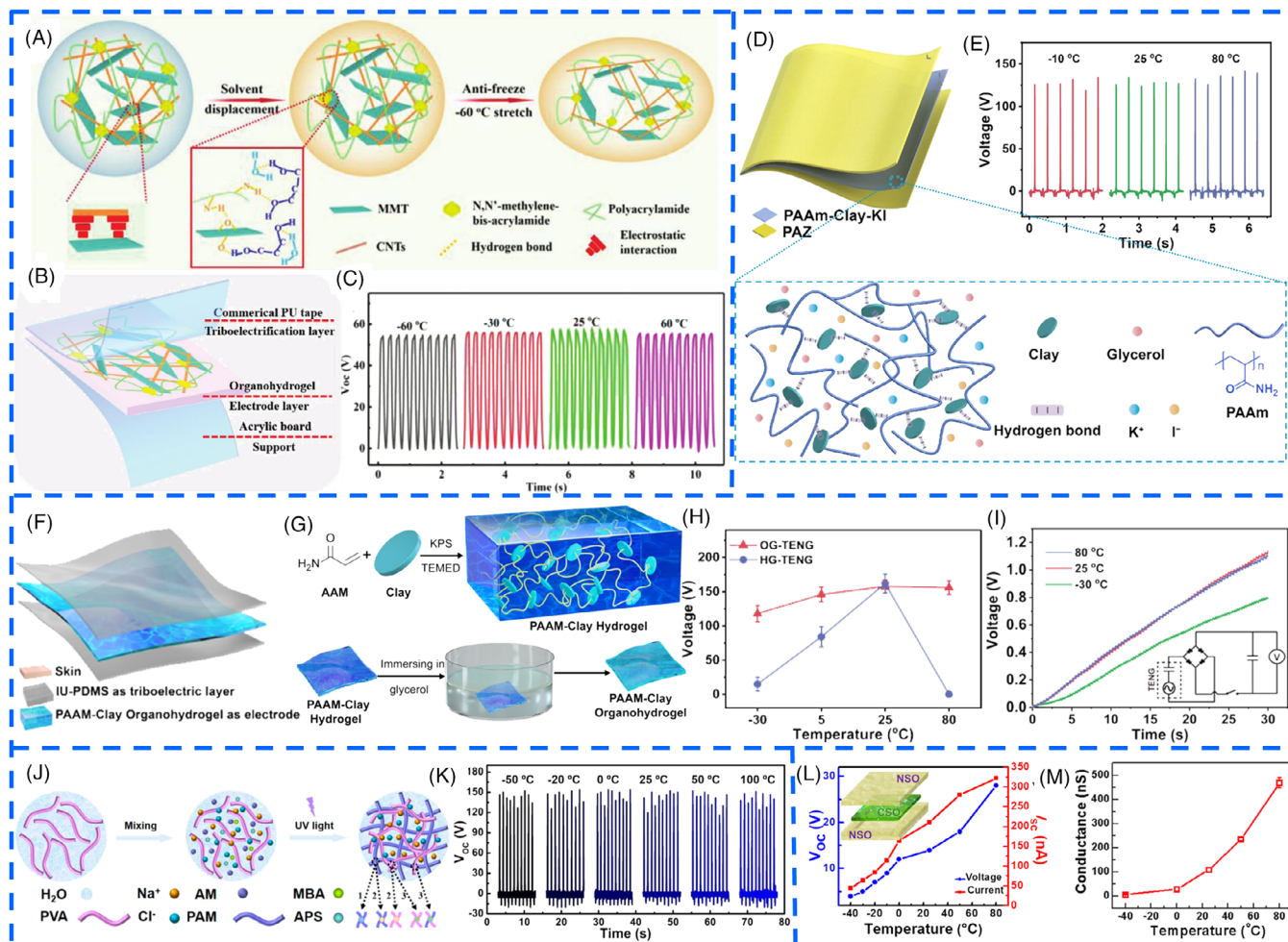


FIGURE 15 (A) Schematic fabrication of environmentally tolerant polyacrylamide/montmorillonite/carbon nanotube organohydrogel (MMCOHs). (B) Structural diagram of the anti-drying organohydrogel-based triboelectric nanogenerator (TENG) (AOH-TENG). (C) V_{oc} of AOH-TENG over a temperature range of -60 to 60°C . (D) Structure of the sandwich-like self-powered sensor device and the chemical composition of PAAM-Clay-KI organohydrogel. (E) V_{oc} of the device following storage at various temperatures. (F) Schematic diagram of organohydrogel-based TENG (OG-TENG). (G) Schematic illustration of PAAM-Clay organohydrogel. (H) V_{oc} versus temperature of the OG-TENG and hydrogel-based TENG (HG-TENG). (I) Voltage profile of a $4.7 \mu\text{F}$ capacitor during charging by the OG-TENG. (J) Synthesis process of PAM/PVA/NaCl (AVN) organohydrogels. (K) V_{oc} of AVN-based organohydrogel-based TENG (OHS-TENG) at different temperatures. (L) The comparative chart of V_{oc} with I_{sc} outputs at different temperatures (inset: structural schematic of the conductive self-healing organohydrogels-based TENG device [CSO-TENG]). (M) Conductance of CSO at different temperatures. *Source:* (A–C) Reproduced with permission from Ref. [169]. Copyright 2021, Wiley-VCH. (D and E) Reproduced with permission from Ref. [170]. Copyright 2022, The Royal Society of Chemistry. (F–I) Reproduced with permission from Ref. [171]. Copyright 2020, Elsevier. (J and K) Reproduced with permission from Ref. [172]. Copyright 2020, American Chemical Society. (L and M) Reproduced with permission from Ref. [173]. Copyright 2021, Elsevier.

researchers because of their exceptional ionic conductivity, robust thermal and chemical stability, non-volatility, and nonflammability.^{180,181} Ionic elastomers, on the other hand, consist entirely of a network of cross-linked polyelectrolytes and associated counter-ions without any liquid component,^{182,183} which makes them naturally resistant to leakage or evaporation. Consequently, both ionogels and ionic elastomers demonstrate remarkable environmental tolerance.

Recently, Liao,¹⁸⁴ Li,¹⁸⁵ Sun,¹⁸⁶ and Zhang et al.,¹²⁶ respectively, constructed TENG devices with a sandwich structure utilizing four different ionogels as electrodes, as depicted in Figure 16C,D and E–L. The ionogels possess excellent chemical and thermal stability, enabling the abovementioned TENG devices to maintain relatively stable electrical outputs across various temperature ranges: -20 to 40 , -30 to 80 , -20 to 100 , and -20 to 110°C , respectively. Additionally, Cheng et al. developed an ionic

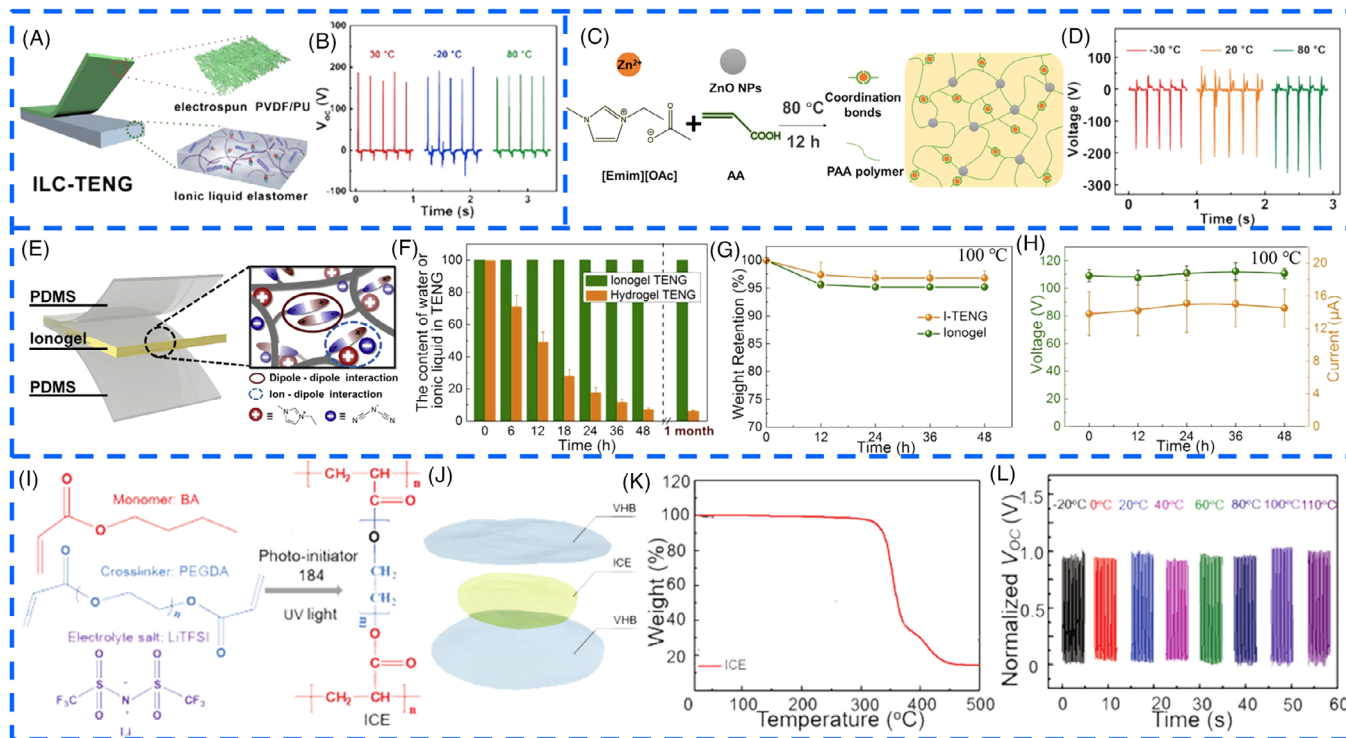


FIGURE 16 (A) Structure diagram of ionic liquid elastomer-based triboelectric nanogenerator (TENG) (ILC-TENG). (B) V_{oc} comparison of ILC-TENG at varying temperatures. (C) Synthesis procedure for PAA-Zn_x/ZnO_m/IL_n ionogels. (D) V_{oc} comparison of self-healing ionogel-based TENG (SI-TENG) at varying temperatures. (E) Scheme of ionogel-based TENG (I-TENG) with a sandwich architecture. (F) The temporal evolution of water or ionic liquid in TENGs. (G) The temporal weight retention of the ionogel and I-TENG. (H) V_{oc} and I_{sc} of the I-TENG with time in a high-temperature environment (30% RH, 100 °C). (I) The manufacturing process of the polymerized ion-conducting elastomer (ICE). (J) Scheme of the sandwich-structured ICE-based ionic TENG (ICE-iTENG). (K) TGA curve of the ICE. (L) Normalized V_{oc} value of the ICE-iTENG measured by contact-separation to a Nylon film at various temperatures. *Source:* (A and B) Reproduced with permission from Ref. [114]. Copyright 2022, Elsevier. (C and D) Reproduced with permission from Ref. [185]. Copyright 2021, Elsevier. (E–H) Reproduced with permission from Ref. [186]. Copyright 2019, Elsevier. (I–L) Reproduced with permission from Ref. [126]. Copyright 2020, Wiley-VCH.

elastomer-based TENG (ILC-TENG) with CNT-doped ILC as the electrode and PVDF/PU nanofibrous membrane as the tribo-layer (Figure 16A,B).¹¹⁴ The TENG devices produced peak-to-peak V_{oc} of 177.44, 182.90, and 179.18 V at –20, 30, and 80 °C, respectively, indicating that the ILC-TENG also maintains stable electrical output characteristic over a wide temperature range.

More significantly, Lu and Zhang et al.^{187,188} independently developed ionic conductive elastomer-based TENG devices utilizing liquid-free cellulose-derived ionic conductive elastomer (ChCl/urea-MCCM_{3%}-AA, Figure 17A,B) and solvent-free elastomeric ionic conductor (TEOA-PTA@LiTFSI, Figure 17E,F) as electrodes. As is widely recognized, the ability of triboelectric devices to maintain their electric output characteristics under extreme conditions is a crucial factor for TENG devices. Notably, as depicted in Figure 17D,H, the electrical outputs of the PDES-TENG and sustainable TENG devices displayed a noticeable increasing trend with rising temperature up to 60 °C, which may be attributed to a

decrease in internal resistance (i.e., an increase in ionic conductivity, Figure 17C,G) of the ChCl/urea-MCCM_{3%}-AA and TEOA-PTA@LiTFSI ionic elastomers at high temperatures.

3.5.3 | Aerogels-based HTO-TENG

Aerogel is a remarkable ultra-lightweight porous material that replaces the liquid component of gel with gas,^{189,190} which is a typical bulk material with nanostructured solid skeletons and open pores, offering excellent physical and chemical properties such as ultra-low density, high porosity, ultrahigh specific surface area, ultra-strong adsorption capacity, and adjustable surface chemistry.^{191,192} These exceptional characteristics make aerogel an ideal material for various applications, offering broad prospects for its use.^{189,190} Recently, the feasibility of aerogel has been widely explored in different fields, showcasing its potential for diverse applications.¹⁹³

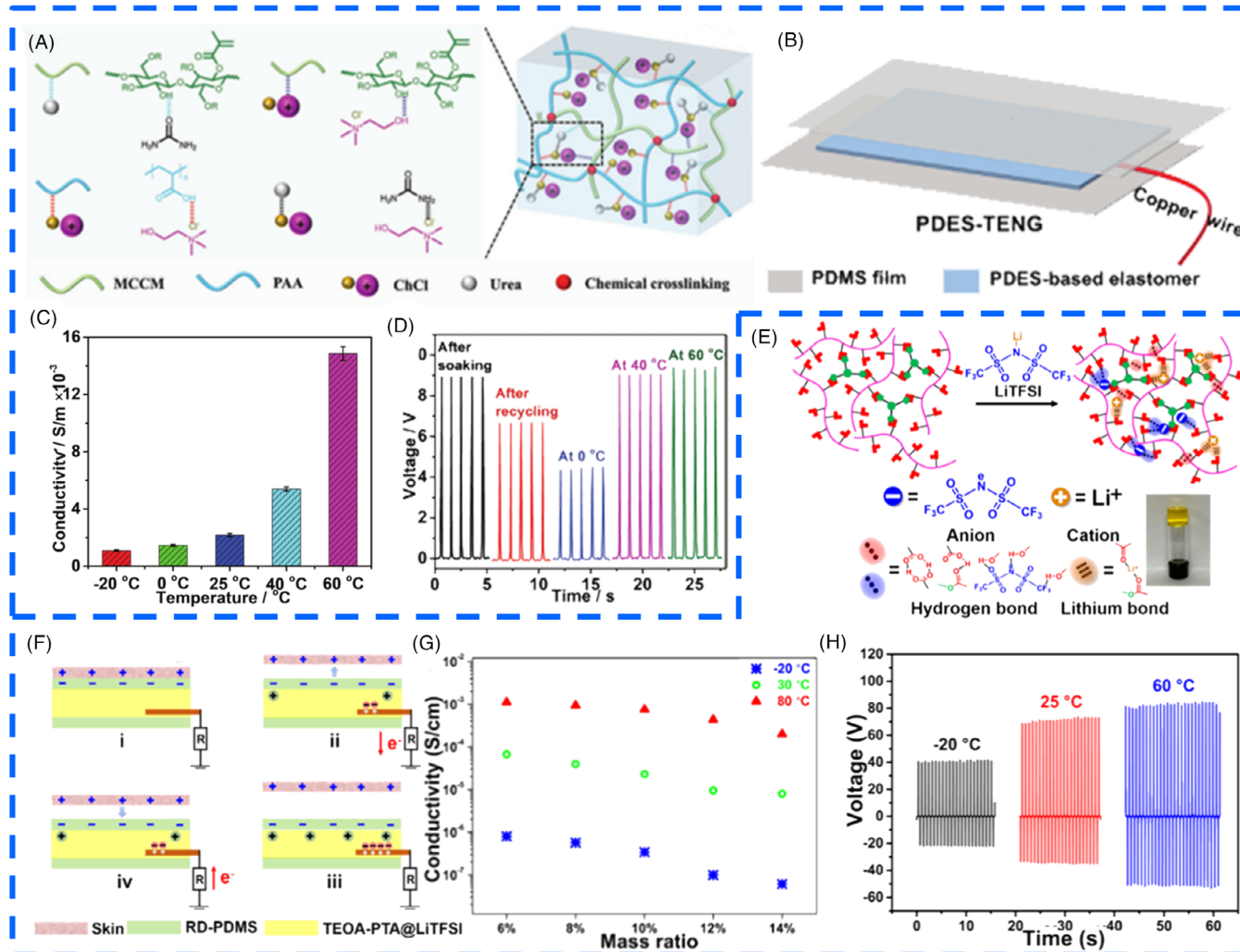


FIGURE 17 (A) Schematic diagram depicting the crosslinking structure of cellulose-derived polymerizable deep eutectic solvents (PDES)-based ionic conductive elastomer. (B) Schematic diagram of the fabricated PDES-triboelectric nanogenerator (TENG). (C) The conductivity of ChCl/urea-MCCM_{3%}-AA (AA, acrylic acid; ChCl, choline chloride, MCCM, cellulose macro-crosslinker,) at various temperatures. (D) The output performance of PDES-TENG under various conditions, including soaking, recycling, and different temperatures. (E) Structure diagram of the elastomeric ionic conductor (TEOA-PTA@LiTFSI). (F) Principles of operation for single-electrode-mode sustainable TENG (SU-TENG). (G) Ionic conductivity of TEOA-PTA@LiTFSI with varying levels of TEOA doping at -20, 30, and 80 °C. (H) V_{oc} of SU-TENG operating at three different temperatures (-20, 25, and 60 °C). *Source:* (A–D) Reproduced with permission from Ref. [187]. Copyright 2022, Wiley-VCH. (E–H) Reproduced with permission from Ref. [188]. Copyright 2022, American Chemical Society.

He et al. utilized a combination of traditional wet spinning technology and emerging triboelectric technology to create an SFA e-textile (Figure 18A) that is based on thermal-induced conductive aerogel fiber (TIC-AF, Figure 18B–D).¹⁹⁴ By incorporating Fe₃O₄ nanoparticles and Ag NWs into calcium alginate-based AFs, the researchers were able to achieve repeatable and highly sensitive temperature monitoring as well as energy harvesting for the SFA e-textile (Figure 18F). The resulting SFA e-textile was then integrated into firefighting protective clothing to provide wide-range temperature sensing and repeatable fire warning capabilities, demonstrating its potential for enhancing the safety of firefighters in

high-risk environments. Although the V_{oc} of the TENG decreased as the temperature increased from 25 to 250 °C (Figure 18G), it still retained 47.7% of its initial electrical output at 250 °C, indicating its high-temperature operability and effective functionality across a wide range of temperature environments.

Flame-retardant electronegative aerogel materials are highly suitable for TENGs operating in extreme environments such as thermal power plants and aerospace.¹⁹⁶ However, the existing electronegative aerogel materials are predominantly polymeric materials that require further enhancement in high-temperature stability and flame resistance. Recently, a series of research explorations

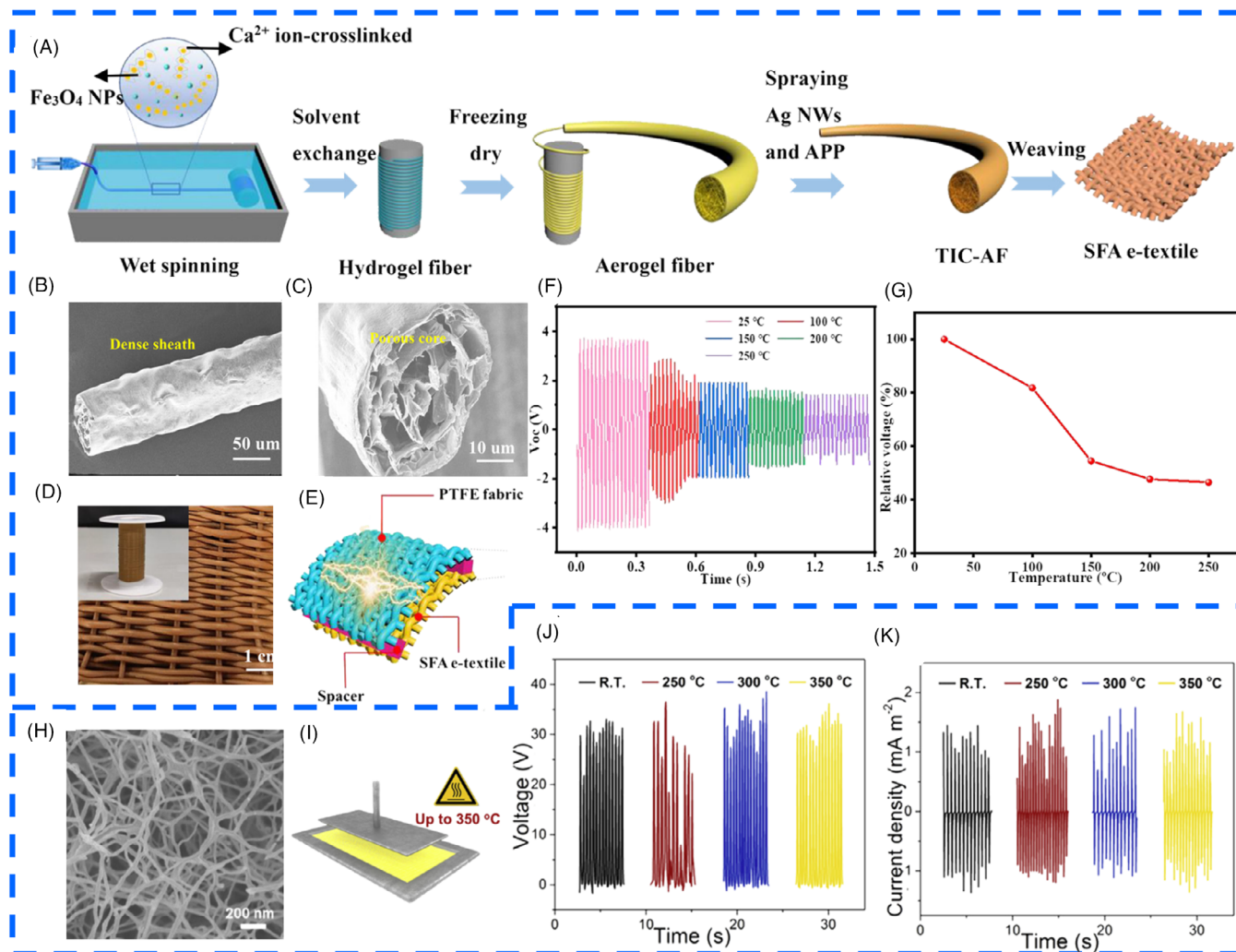


FIGURE 18 (A) The production of thermal-induced conductive aerogel fiber (TIC-AF) and self-powered fire alarm electronic textile (SFA e-textile). Surface (B) and cross-sectional (C) SEM images of TIC-AF. (D) Photograph of SFA e-textile woven from TIC-AFs. (E) Schematic diagram of the as-prepared triboelectric nanogenerator (TENG) by integrating the SFA e-textile and polytetrafluoroethylene (PTFE) material. (F) V_{oc} of the SFA e-textile-based TENG across a wide temperature range. (G) Relative voltage of the TENG under different temperature conditions. (H) SEM images of the compressed poly(*p*-phenylene benzobisoxazole) aerogel (PBOA) films. (I) Schematic depiction of PBOA/Al TENGs. (J) V_{oc} and (K) current density of PBOA/Al TENGs performed at various temperatures. *Source:* (A–G) Reproduced with permission from Ref. [194]. Copyright 2022, American Chemical Society. (H–K) Reproduced with permission from Ref. [195]. Copyright 2019, Elsevier.

have been conducted in this field. For instance, Qian et al. fabricated poly(*p*-phenylene benzobisoxazole) aerogels (PBOAs) (Figure 18H) from poly(*p*-phenylene benzobisoxazole) fibers and used it utilized them as the electronegative tribo-materials.¹⁹⁵ Subsequently, the as-fabricated PBOA was paired with Al foil to construct PBOA/Al TENGs (Figure 18I). As demonstrated in Figure 18J,K, the electrical output performance of the as-constructed PBOA/Al TENGs remained almost unaffected within the temperature range of room temperature to 350°C. Moreover, these PBOA/Al TENGs exhibited a V_{oc} of 32 V, and a J_{sc} of 1.2 mA m⁻² even at high temperatures up to 350°C, demonstrating the potential for

application of triboelectrical devices in high-temperature environments.

3.6 | Metal-organic frameworks (MOF)-based HTO-TENG

MOFs are a type of crystalline porous materials consisting of metal ions (or clusters) with multifunctional organic ligands.^{197–199} Due to their porous feature, highly ordered structure, and ability to be rationally designed and assembled for desired versatility, they have been widely used in energy conversion and storage applications.^{200–202} Among

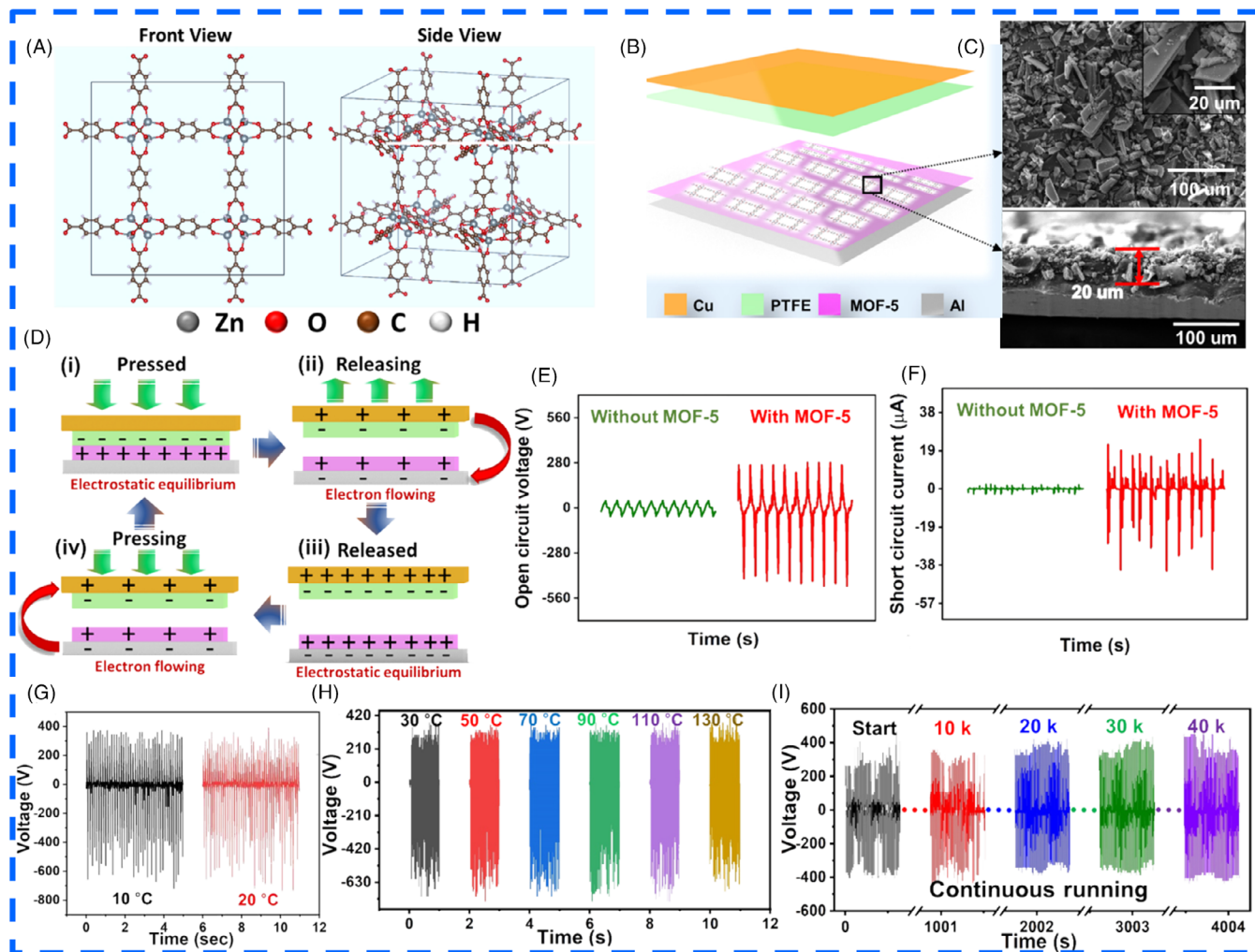


FIGURE 19 (A) The crystalline structure of metal–organic framework (MOF)-5. (B) Schematic illustration of MOF-5-based triboelectric nanogenerator (TENG) device. (C) Surface and cross-sectional SEM images of MOF-5 film. (D) Operational mechanism of MOF-5-based TENG device. (E) V_{oc} and (F) I_{sc} of the TENG devices without and with MOF-5. (G) V_{oc} of MOF-5-based TENG device at low temperatures (such as 10 and 20 °C). (H) V_{oc} of MOF-5-based TENG device by hand slapping at various temperatures. (I) Stability assessment of MOF-5-based TENG device. *Source:* Reproduced with permission from Ref. [32]. Copyright 2022, Elsevier.

different types of MOFs, isoreticular MOFs (IRMOFs), a subfamily of MOFs with exceptional thermal and chemical stability, tunable porosity, and high surface area,^{32,203} hold great potential for fabricating ultra-durable triboelectric and piezoelectric nanogenerators with superior environmental stability. In a recent study by Shaukat et al., an MOF (MOF-5 or IRMOF-1) was used for the first time to fabricate a TENG for energy harvesting, as illustrated in Figure 19A–D.³² The TENG based on MOF-5 demonstrated excellent electrical outputs (Figure 19E,F) including V_{oc} of 484 V, I_{sc} of 40 μA , and maximum instantaneous power of 3174 μW . Furthermore, the as-constructed TENG exhibited stable output performances under untoward environmental conditions such as temperature variations ranging from -10 to 130 °C (Figure 19G–I), demonstrating its robustness under challenging operational environmental. These find-

ings suggest that MOF-5 is a highly promising alternative for constructing ultra-robust TENGs that can operate at high temperatures.

4 | CONCLUSIONS AND OUTLOOK

With the increasing demand for energy in scientific missions and extreme environments, HTO-TENGs have demonstrated extensive potential applications in self-powered microelectronics technologies under extreme climate conditions (such as sensor networks and oil exploration equipment), energy harvesting and conversion in high-temperature industrial processes, aerospace fields, and self-sustained wireless sensor networks in hot environments. The efficient triboelectric energy harvesting at

high temperatures has become a critical research area. It is imperative and timely to comprehensively evaluate the progress made thus far in creating self-powered power source systems that are sustainable, self-sufficient, durable, and capable of operating effectively even when exposed to elevated temperatures. This review thoroughly discusses the current research status and advancements of HTO-TENG devices while emphasizing that developing triboelectric functional layers with outstanding heat resistance, stability, durability, stable dielectric performance, and effectively suppressing or overcoming the electron thermionic emission effect is pivotal for constructing HTO-TENG devices. However, despite the recent surge in HTO-TENG manufacturing, there are still some prominent challenges that require further attention and resolution.

- (1) The continuous improvement of TENG's output performance serves as a driving force for sustainable development. First, high-temperature environments pose higher demands on material performance, necessitating the use of materials that maintain stability and performance under high temperatures for TENGs. Second, under such conditions, enhanced electron thermionic emission effects may interfere with normal charge collection. Effectively suppressing or overcoming this effect is one of the challenges in the design of TENGs. Furthermore, the mechanical stability of these generators is also challenged at high temperatures, requiring device design to maintain structural integrity under extreme conditions. Lastly, increased temperature may result in unstable energy output which is unacceptable in certain applications. In subsequent research, it is anticipated that a manufacturing technique for HTO-TENG devices can be developed to significantly enhance power output, particularly in terms of current and power density, by comprehensively considering the aforementioned four aspects.
- (2) As the demand for self-powered wearable electronic devices continues to increase, there is a growing need to manufacture HTO-TENG devices with improved wear resistance, higher temperature limits, and diversified functions such as softness, permeability, biocompatibility, flame retardancy, self-healing capabilities, and thermal management abilities. These improvements will contribute to the rapid advancement of this field and broaden its application scope.
- (3) The operating mechanism of HTO-TENGs is currently unclear. To provide guidance for exploring new manufacturing strategies, more comprehensive research should be conducted on the intrinsic operating mechanism of HTO-TENGs in subsequent studies.

Additionally, it is also necessary to develop an evaluation standard for the triboelectric performance of HTO-TENGs.

- (4) The future large-scale practical application of self-powered electronic devices in extreme environments necessitates the large-scale production and industrialization of HTO-TENGs with exceptional performance.

In summary, there is an urgent need to develop more advanced manufacturing strategies for the production of HTO-TENGs with enhanced performance and multifunctional integration. Exploring effective mechanisms to suppress or overcome the inherent electron thermionic emission effect will provide valuable theoretical guidance for future research on efficient and multifunctional HTO-TENGs, further promoting the rapid development and practical application of this field. Further, overcoming the challenges in high-temperature environments will enable triboelectric devices to demonstrate broad prospects for applications in various fields, thereby bringing new possibilities for self-powering technology and energy conversion.

ACKNOWLEDGMENTS

This work was supported by the National Natural Science Foundation of China (No. 52003074, 52125205, U20A20166, 52192614, 52003073, and 62174049), the Project funded by China Postdoctoral Science Foundation (No. 2020M680097), the Postdoctoral Fellowship Program of CPSF (No. GZC20230681), the Natural Science Foundation of Henan Province (No. 202300410058), the National Science Fund for Excellent Young Scholars of Henan Province (No. 222300420033), National key R&D program of China (2021YFB3200302 and 2021YFB3200304), Natural Science Foundation of Beijing Municipality (Z180011 and 2222088), Shenzhen Science and Technology Program (grant number KQTD20170810105439418), and the Fundamental Research Funds for the Central Universities.

CONFLICT OF INTEREST STATEMENT

The authors declare no conflict of interest.

ORCID

Caiqin Luo  <https://orcid.org/0000-0003-4368-0627>

Caofeng Pan  <https://orcid.org/0000-0001-6327-9692>

REFERENCES

1. Su YJ, Chen J, Wu ZM, Jiang YD. Low temperature dependence of triboelectric effect for energy harvesting and self-powered active sensing. *Appl Phys Lett*. 2015;106:013114.
2. Chao SY, Ouyang H, Jiang DJ, Fan YB, Li Z. Triboelectric nanogenerator based on degradable materials. *Ecomat*. 2021;3:e12072.

3. Yu DJ, Wang P, Cao F, et al. Two-dimensional halide perovskite as β -ray scintillator for nuclear radiation monitoring. *Nat Commun.* 2020;11:3395.
4. Lu CX, Han CB, Gu GQ, et al. Temperature effect on performance of triboelectric nanogenerator. *Adv Eng Mater.* 2017;19:1700275.
5. Hou S, Chen L, Fan XL, et al. High-energy and low-cost membrane-free chlorine flow battery. *Nat Commun.* 2022;13:1281.
6. Chen X, Li ML, Wang SP, et al. In situ fabrication of cuprous selenide electrode via selenization of copper current collector for high-efficiency potassium-ion and sodium-ion storage. *Adv Sci.* 2022;9:2104630.
7. Tian Y, An YL, Xu BG. MXene-based materials for advanced nanogenerators. *Nano Energy.* 2022;101:107556.
8. Chen AH, Zhang C, Zhu G, Wang ZL. Polymer materials for high-performance triboelectric nanogenerators. *Adv Sci.* 2020;7:2000186.
9. Zhang Q, Zhang ZX, Liang QJ, Shi QF, Zhu ML, Lee CK. All in one, self-powered bionic artificial nerve based on a triboelectric nanogenerator. *Adv Sci.* 2021;8:2004727.
10. Lone SA, Lim KC, Kaswan K, et al. Recent advancements for improving the performance of triboelectric nanogenerator devices. *Nano Energy.* 2022;99:107318.
11. Dong K, Deng JN, Zi YL, et al. 3D orthogonal woven triboelectric nanogenerator for effective biomechanical energy harvesting and as self-powered active motion sensors. *Adv Mater.* 2017;29:1702648.
12. Sun MZ, Lu QY, Wang ZL, Huang BL. Understanding contact electrification at liquid-solid interfaces from surface electronic structure. *Nat Commun.* 2021;12:1752.
13. La JX, i, Ke Y, Cao ZK, et al. Bimetallic strip based triboelectric nanogenerator for self-powered high temperature alarm system. *Nano Today.* 2022;43:101437.
14. Tang Y, Xu BG, Gao YY, et al. Ultrastrong-polar polyacrylonitrile organic-inorganic architected nanogenerators with synergistic triboelectric behavior for efficient biomechanical energy harvesting and self-powered sensing. *Nano Energy.* 2022;103:107833.
15. Kim Y, Lee D, Seong J, Bak B, Choi UH, Kim J. Ionic liquid-based molecular design for transparent, flexible, and fire-retardant triboelectric nanogenerator (TENG) for wearable energy solutions. *Nano Energy.* 2021;84:105925.
16. Wu CS, Wang AC, Ding WB, Guo HY, Wang ZL. Triboelectric nanogenerator: a foundation of the energy for the new era. *Adv Energy Mater.* 2019;9:1802906.
17. Barman SR, Chan S-W, Kao F-C, et al. A self-powered multifunctional dressing for active infection prevention and accelerated wound healing. *Sci Adv.* 2023;9:eadc8758.
18. Luo JJ, Shi X, Chen PF, et al. Strong and flame-retardant wood-based triboelectric nanogenerators toward self-powered building fire protection. *Mater Today Phys.* 2022;27:100798.
19. Ouyang H, Liu Z, Li N, et al. Symbiotic cardiac pacemaker. *Nat Commun.* 2019;10:1821.
20. Guan QB, Lu X, Chen YY, et al. High-performance liquid crystalline polymer for intrinsic fire-resistant and flexible triboelectric nanogenerators. *Adv Mater.* 2022;34:2204543.
21. Barman SR, Lin Y-J, Lee K-M, et al. Triboelectric nanosensor integrated with robotic platform for self-powered detection of chemical analytes. *ACS Nano.* 2023;17:2689-2701.
22. Chen Y-H, Lin P-Y, Wang T-W, et al. Dynamics of electrically driven cholesteric liquid crystals by triboelectrification and their application in self-powered information securing and vision correcting. *ACS Energy Lett.* 2021;6:3185-3194.
23. Xu C, Zi YL, Wang AC, et al. On the electron-transfer mechanism in the contact-electrification effect. *Adv Mater.* 2018;30:1706790.
24. Wang AC, Zhang BB, Xu C, Zou HY, Lin ZQ, Wang ZL. Unraveling temperature-dependent contact electrification between sliding-mode triboelectric pairs. *Adv Funct Mater.* 2020;30:1909384.
25. Xu C, Wang AC, Zou HY, et al. Raising the working temperature of a triboelectric nanogenerator by quenching down electron thermionic emission in contact-electrification. *Adv Mater.* 2018;30:1803968.
26. Wang R, Ji MM, Jin X, Zhang QR, Jiao TF. Recent developments in functional triboelectric nanogenerators for flame-retardant, human health, and energy-harvesting fields: a crucial review. *Nano Futures.* 2022;6:022003.
27. Cheng BL, Xu Q, Ding YQ, et al. High performance temperature difference triboelectric nanogenerator. *Nat Commun.* 2021;12:4782.
28. Tan CX, Dong ZG, Li YH, et al. A high performance wearable strain sensor with advanced thermal management for motion monitoring. *Nat Commun.* 2020;11:3530.
29. Wu J-P, Liang W, Song W-Z, et al. An acid and alkali-resistant triboelectric nanogenerator. *Nanoscale.* 2020;12:23225-23233.
30. Chougale MY, Saqib QM, Khan MU, Shaikat RA, Kim J, Bae J. Novel recycled triboelectric nanogenerator based on polymer-coated trash soda can for clean energy harvesting. *Adv Sustainable Syst.* 2021;5:2100161.
31. Zhang P, Zhang WK, Deng L, Zhang HH. A triboelectric nanogenerator based on temperature-stable high dielectric BaTiO₃-based ceramic powder for energy harvesting. *Nano Energy.* 2021;87:106176.
32. Shaikat RA, Saqib QM, Kim J, et al. Ultra-robust tribo- and piezo-electric nanogenerator based on metal organic frameworks (MOF-5) with high environmental stability. *Nano Energy.* 2022;96:107128.
33. Bui VT, Oh JH, Kim JN, Zhou QT, Huynh DP, Oh IK. Nest-inspired nanosponge-Cu woven mesh hybrid for ultrastable and high-power triboelectric nanogenerator. *Nano Energy.* 2020;71:104561.
34. Kim D, Lee S, Ko Y, Kwon CH, Cho J. Layer-by-layer assembly-induced triboelectric nanogenerators with high and stable electric outputs in humid environments. *Nano Energy.* 2018;44:228-239.
35. Pandey RK, Ao CK, Lim W, et al. The relationship between static charge and shape. *ACS Cent Sci.* 2020;6:704-714.
36. Li SM, Zhou YS, Zi YL, Zhang G, Wang ZL. Excluding contact electrification in surface potential measurement using Kelvin probe force microscopy. *ACS Nano.* 2016;10:2528-2535.
37. Lin SQ, Xu L, Xu C, et al. Electron transfer in nanoscale contact electrification: effect of temperature in the metal-dielectric case. *Adv Mater.* 2019;31:1808197.

38. Wang ZL, Wang AC. On the origin of contact-electrification. *Mater Today*. 2019;30:34-51.
39. Seol M-L, Han J-W, Moon D-I, Meyyappan M. Triboelectric nanogenerator for Mars environment. *Nano Energy*. 2017;39:238-244.
40. Zhao ZF, Pu X, Du CH, et al. Freestanding flag-type triboelectric nanogenerator for harvesting high-altitude wind energy from arbitrary directions. *ACS Nano*. 2016;10:1780-1787.
41. Zhao YJ, Shen SW, Cao RR, et al. Flexible stretchable tribo-negative films with exceptional output performance for high-temperature energy harvesting and self-powered sensor. *Nano Energy*. 2023;114:108654.
42. Tao XL, Li SY, Shi YX, et al. Triboelectric polymer with high thermal charge stability for harvesting energy from 200°C flowing air. *Adv Funct Mater*. 2021;31:2106082.
43. Wen XN, Su YJ, Yang Y, Zhang HL, Wang ZL. Applicability of triboelectric generator over a wide range of temperature. *Nano Energy*. 2014;4:150-156.
44. Cheng RW, Dong K, Liu LX, et al. Flame-retardant textile-based triboelectric nanogenerators for fire protection applications. *ACS Nano*. 2020;14:15853-15863.
45. Shi FL, Wei X, Wang HC, Wu XQ. Electrospun polyimide nanofiber-based triboelectric nanogenerator for harvesting energy at elevated temperatures. *ACS Appl Electron Mater*. 2022;4(9):4569-4575.
46. Su L, Wang HL, Tian Z, Wang HJ, Cheng Q, Yu W. Low detection limit and high sensitivity wind speed sensor based on triboelectrification-induced electroluminescence. *Adv Sci*. 2019;6:1901980.
47. Zhang BS, Gao Q, Li WB, et al. Alternating magnetic field-enhanced triboelectric nanogenerator for low-speed flow energy harvesting. *Adv Funct Mater*. 2023;33:2304839.
48. Han JJ, Liu Y, Feng YW, Jiang T, Wang ZL. Achieving a large driving force on triboelectric nanogenerator by wave-driven linkage mechanism for harvesting blue energy toward marine environment monitoring. *Adv Energy Mater*. 2022;13:2203219.
49. Almuslem AS, Shaikh SF, Hussain MM. Flexible and stretchable electronics for harsh-environmental applications. *Adv Mater Technol*. 2019;4:1900145.
50. Niu Y, Liu H, He RY, et al. The new generation of soft and wearable electronics for health monitoring in varying environment: from normal to extreme conditions. *Mater Today*. 2020;41:219-242.
51. Xing FJ, Ou ZQ, Gao XB, Chen BD, Wang ZL. Harvesting electrical energy from high temperature environment by aerogel nano-covered triboelectric yarns. *Adv Funct Mater*. 2022;32:2205275.
52. Liu D, Gao YK, Zhou LL, Wang J, Wang ZL. Recent advances in high-performance triboelectric nanogenerators. *Nano Res*. 2023;16:11698-11717.
53. Du TL, Dong FY, Xi ZY, et al. Recent advances in mechanical vibration energy harvesters based on triboelectric nanogenerators. *Small*. 2023;19:2300401.
54. Zhang Q, Xin CF, Shen F, et al. Human body IoT systems based on the triboelectrification effect: energy harvesting, sensing, interfacing and communication. *Energy Environ Sci*. 2022;15:3688-3721.
55. Wang Z. From contact electrification to triboelectric nanogenerators. *Rep Prog Phys*. 2021;84:096502.
56. Shan CC, Liu WL, Wang Z, et al. An inverting TENG to realize the AC mode based on the coupling of triboelectrification and air-breakdown. *Energy Environ Sci*. 2021;14:5395-5405.
57. Zhou YS, Li SM, Niu SM, Wang ZL. Effect of contact- and sliding-mode electrification on nanoscale charge transfer for energy harvesting. *Nano Res*. 2016;9:3705-3713.
58. Zhou YS, Wang SH, Yang Y, et al. Manipulating nanoscale contact electrification by an applied electric field. *Nano Lett*. 2014;14(3):1567-1572.
59. Wang ZL. On Maxwell's displacement current for energy and sensors: the origin of nanogenerators. *Mater Today*. 2017;20(2):74-82.
60. Choi D, Lee Y, Lin ZH, et al. Recent advances in triboelectric nanogenerators: from technological progress to commercial applications. *ACS Nano*. 2023;17(12):11087-11219.
61. Wang ZL. On the first principle theory of nanogenerators from Maxwell's equations. *Nano Energy*. 2020;68:104272.
62. Elsanadidy E, Mosa IM, Luo D, et al. Advances in triboelectric nanogenerators for self-powered neuromodulation. *Adv Funct Mater*. 2023;33:2211177.
63. Li H, Sinha TK, Oh JS, et al. Soft and flexible bilayer thermoplastic polyurethane foam for development of bioinspired artificial skin. *ACS Appl Mater Interfaces*. 2018;10(16):14008-14016.
64. Ren XH, Xiang XY, Yin HF, Tang Y, Yuan HD. All-yarn triboelectric nanogenerator and supercapacitor based self-charging power cloth for wearable applications. *Nanotechnology*. 2021;32:315404.
65. Ma WT, Zhang MQ, Yan W, Zhu JB, Liu JZ, Song WX. Ultraviolet self-charging triboelectric power paper with enhanced on-chip energy storage. *Nano Energy*. 2022;101:107601.
66. Wen J, Chen BD, Tang W, et al. Harsh-environmental-resistant triboelectric nanogenerator and its applications in autodrive safety warning. *Adv Energy Mater*. 2018;8:1801898.
67. Zhang SL, Lai Y-C, He X, Liu RY, Zi YL, Wang ZL. Auxetic foam-based contact-mode triboelectric nanogenerator with highly sensitive self-powered strain sensing capabilities to monitor human body movement. *Adv Funct Mater*. 2017;27:1606695.
68. Wang SH, Xie YN, Niu SM, Lin L, Wang ZL. Freestanding triboelectric-layer-based nanogenerators for harvesting energy from a moving object or human motion in contact and non-contact modes. *Adv Mater*. 2014;26:2818-2824.
69. He WC, Liu WL, Chen J, et al. Boosting output performance of sliding mode triboelectric nanogenerator by charge space-accumulation effect. *Nat Commun*. 2020;11:4606.
70. Niu SM, Liu Y, Wang SH, et al. Theory of sliding-mode triboelectric nanogenerators. *Adv Mater*. 2013;25:6184-6193.
71. Zhou LL, Liu D, Li SX, et al. Rationally designed dual-mode triboelectric nanogenerator for harvesting mechanical energy by both electrostatic induction and dielectric breakdown effects. *Adv Energy Mater*. 2020;10:2000965.
72. Xu HB, Kim JH, Kim S, et al. Double layered dielectric elastomer by vapor encapsulation casting for highly deformable and strongly adhesive triboelectric materials. *Nano Energy*. 2019;62:144-153.
73. Niu SM, Wang ZL. Theoretical systems of triboelectric nanogenerators. *Nano Energy*. 2015;14:161-192.

74. Wang ZL, Chen J, Lin L. Progress in triboelectric nanogenerators as a new energy technology and self-powered sensors. *Energy Environ Sci.* 2015;8:2250-2282.
75. Duan QS, Zhang ZJ, Zhao JM, et al. Fire-retardant hydroxypapatite/cellulosic triboelectric materials for energy harvesting and sensing at extreme conditions. *Nano Energy.* 2023;117:108851.
76. Zhong XD, Sun P, Wei RC, Dong HR, Jiang SH. Object recognition by a heat-resistant core-sheath triboelectric nanogenerator sensor. *J Mater Chem A.* 2022;10:15080-15088.
77. Ye C, Yang S, Ren J, et al. Electroassisted core-spun triboelectric nanogenerator fabrics for IntelliSense and artificial intelligence perception. *ACS Nano.* 2022;16(3):4415-4425.
78. Dong K, Deng JN, Ding WB, et al. Versatile core-sheath yarn for sustainable biomechanical energy harvesting and real-time human-interactive sensing. *Adv Energy Mater.* 2018;8:180114.
79. Zhou MJ, Xu F, Ma LY, et al. Continuously fabricated nano/micro aligned fiber based waterproof and breathable fabric triboelectric nanogenerators for self-powered sensing systems. *Nano Energy.* 2022;104:107885.
80. Zhang C, Chen JK, Xuan WP, et al. Conjunction of triboelectric nanogenerator with induction coils as wireless power sources and self-powered wireless sensors. *Nat Commun.* 2020;11:58.
81. Yang YQ, Guo XG, Zhu ML, et al. Triboelectric nanogenerator enabled wearable sensors and electronics for sustainable internet of things integrated green earth. *Adv Energy Mater.* 2022;13:2203040.
82. Shao ZC, Chen JS, Gao KX, et al. A double-helix metal-chain metal-organic framework as a high-output triboelectric nanogenerator material for self-powered anticorrosion. *Angew Chem Int Ed.* 2022;61:e202208994.
83. Wu J, Xi YH, Shi YJ. Toward wear-resistive, highly durable and high performance triboelectric nanogenerator through interface liquid lubrication. *Nano Energy.* 2020;72:104659.
84. Ryu H, Park HM, Kim MK, et al. Self-rechargeable cardiac pacemaker system with triboelectric nanogenerators. *Nat Commun.* 2021;12:4374.
85. Shi L, Jin H, Dong SR, et al. High-performance triboelectric nanogenerator based on electrospun PVDF-graphene nanosheet composite nanofibers for energy harvesting. *Nano Energy.* 2021;80:105599.
86. Bhatta T, Maharjan P, Cho H, et al. High-performance triboelectric nanogenerator based on MXene functionalized polyvinylidene fluoride composite nanofibers. *Nano Energy.* 2021;81:105670.
87. Gu GQ, Han CB, Lu CX, et al. Triboelectric nanogenerator enhanced nanofiber air filters for efficient particulate matter removal. *ACS Nano.* 2017;11(6):6211-6217.
88. Qian JC, He J, Qian S, et al. A nonmetallic stretchable nylon-modified high performance triboelectric nanogenerator for energy harvesting. *Adv Funct Mater.* 2019;30(4):1907414.
89. Mathew DT, Vijoy KV, Nayar NV, et al. Surface area enhanced nylon-6,6 nanofiber engineered triboelectric nanogenerator for self-powered seat monitoring applications. *ACS Sustainable Chem Eng.* 2022;10(43):14126-14135.
90. Sun Y, Zheng YD, Wang R, et al. 3D micro-nanostructure based waterproof triboelectric nanogenerator as an outdoor adventure power source. *Nano Energy.* 2022;100:107506.
91. Pandey P, Thapa K, Ojha GP, et al. Metal-organic frameworks-based triboelectric nanogenerator powered visible light communication system for wireless human-machine interactions. *Chem Eng J.* 2023;452:139209.
92. Gao YY, Liu GX, Bu TZ, et al. MXene based mechanically and electrically enhanced film for triboelectric nanogenerator. *Nano Res.* 2021;14:4833-4840.
93. Wu ZY, Ding WB, Dai YJ, et al. Self-powered multifunctional motion sensor enabled by magnetic-regulated triboelectric nanogenerator. *ACS Nano.* 2018;12(6):5726-5733.
94. Kang CW, Lee DM, Park J, Bang S, Kim SW, Son SU. Core-shell ZnO@microporous organic polymer nanospheres as enhanced piezo-triboelectric energy harvesting materials. *Angew Chem Int Ed.* 2022;61:e202209659.
95. Xiang HJ, Zeng YM, Huang XM, Wang N, Cao X, Wang ZL. From triboelectric nanogenerator to multifunctional triboelectric sensors: a chemical perspective toward the interface optimization and device integration. *Small.* 2022;18:2107222.
96. Šutka A, Mālnieks K, Lapčinskis L, Timusk M, Pudzs K, Rutkis M. Matching the directions of electric fields from triboelectric and ferroelectric charges in nanogenerator devices for boosted performance. *iScience.* 2020;23(4):101011.
97. Sie EJ, Rohwer T, Lee C, Gedik N. Time-resolved XUV ARPES with tunable 24–33 eV laser pulses at 30 meV resolution. *Nat Commun.* 2019;10:3535.
98. Kim M, Park D, Alam MM, Lee S, Park P, Nah J. Remarkable output power density enhancement of triboelectric nanogenerators via polarized ferroelectric polymers and bulk MoS₂ composites. *ACS Nano.* 2019;13(4):4640-4646.
99. Guo FM, Shen X, Zhou JM, et al. Highly thermally conductive dielectric nanocomposites with synergistic alignments of graphene and boron nitride nanosheets. *Adv Funct Mater.* 2020;30:1910826.
100. Ding YF, Shi YX, Nie JH, et al. Thermochromic triboelectric nanogenerator enabling direct visualization of temperature change during operation. *Chem Eng J.* 2020;388:124369.
101. Wang ZL. Triboelectric nanogenerators as new energy technology for self-powered systems and as active mechanical and chemical sensors. *ACS Nano.* 2013;7(11):9533-9557.
102. Kučera M, Láníková J. Thermal stability of polydimethylsiloxane. II. Formation of stable complexes on basic active centers. *J Polym Sci.* 1962;59:79-85.
103. Ma C, Yu B, Hong NN, Pan Y, Hu WZ, Hu Y. Facile synthesis of a highly efficient, halogen-free, and intumescent flame retardant for epoxy resins: thermal properties, combustion behaviors, and flame-retardant mechanisms. *Ind Eng Chem Res.* 2016;55(41):10868-10879.
104. Sullivan A, Saigal A, Zimmerman M. Investigation of liquid crystal polymer structure-property relationships between crystal orientation and dielectric behavior. *J Phys: Conf Series.* 2018;1045:012005.
105. Bui V-T, Chau NM, Huynh DP, Huynh ND, Choi D, Do HN. Honeycomb-patterned polyimide-based triboelectric nanogenerator with excellent thermal stability and enhanced electrification performance. *ACS Appl Energy Mater.* 2022;5:9791-9800.
106. Bui V-T, Huynh ND, Chau NM, et al. High-temperature operable triboelectric nanogenerator using microdome-patterned polyimide for self-powered sensors. *Nano Energy.* 2022;101:107612.

107. Lee CJ, Choi AY, Choi C, Sim HJ, Kim SJ, Kim YT. Triboelectric generator for wearable devices fabricated using a casting method. *RSC Adv.* 2016;6:10094-10098.
108. Jing TT, Xu BG, Yang YJ, Jiang CHZ, Wu MJ. Interfacial modification boosted permittivity and triboelectric performance of liquid doping composites for high-performance flexible triboelectric nanogenerators. *Nano Energy.* 2020;78:105374.
109. Wu SH, Li G, Liu WX, et al. Fabrication of polyethyleneimine-paper composites with improved tribopositivity for triboelectric nanogenerators. *Nano Energy.* 2022;93:106859.
110. Sun Q-J, Lei YQ, Zhao X-H, et al. Scalable fabrication of hierarchically structured graphite/polydimethylsiloxane composite films for large-area triboelectric nanogenerators and self-powered tactile sensing. *Nano Energy.* 2021;80:105521.
111. Li ZH, Xu BG, Han J, Huang JX, Chung KY. Interfacial polarization and dual charge transfer induced high permittivity of carbon dots-Based composite as humidity-resistant tribomaterial for efficient biomechanical energy harvesting. *Adv Energy Mater.* 2021;11:2101294.
112. Zhang RY, Örtengren J, Hummelgård M, Olsen M, Andersson H, Olin H. A review of the advances in composites/nanocomposites for triboelectric nanogenerators. *Nanotechnology.* 2022;33:212003.
113. Cui NY, Gu L, Lei YM, et al. Dynamic behavior of the triboelectric charges and structural optimization of the friction layer for a triboelectric nanogenerator. *ACS Nano.* 2016;10(6):6131-6138.
114. Cheng Y, Zhu WD, Lu XF, Wang C. Mechanically robust, stretchable, autonomously adhesive, and environmentally tolerant triboelectric electronic skin for self-powered healthcare monitoring and tactile sensing. *Nano Energy.* 2022;102:107636.
115. Chen XS, Yusuf A, Rio JSD, Wang DY. A facile and robust route to polyvinyl alcohol-based triboelectric nanogenerator containing flame-retardant polyelectrolyte with improved output performance and fire safety. *Nano Energy.* 2021;81:105656.
116. Chen H, Zhou JY, Liu S, Wang S, Gong XL. Flame-retardant triboelectric generator with stable thermal-mechanical-electrical coupling performance for fire Bluetooth alarm system. *Nano Energy.* 2022;102:107634.
117. Liu ZQ, Huang YZ, Shi YX, et al. Fabrication of triboelectric polymer films via repeated rheological forging for ultrahigh surface charge density. *Nat Commun.* 2022;13:4083.
118. Li ZH, Xu BG, Han J, Huang JX, Fu H. A polycation-modified nanofillers tailored polymer electrolytes fiber for versatile biomechanical energy harvesting and full-range personal healthcare sensing. *Adv Funct Mater.* 2022;32:2106731.
119. Cheng Y, Lu X, Chan KH, et al. A stretchable fiber nanogenerator for versatile mechanical energy harvesting and self-powered full-range personal healthcare monitoring. *Nano Energy.* 2017;41:511-518.
120. Cao RR, Xia YF, Wang J, et al. Suppressing thermal negative effect and maintaining high-temperature steady electrical performance of triboelectric nanogenerators by employing phase change material. *ACS Appl Mater Interfaces.* 2021;13(35):41657-41668.
121. Shen SW, Zhao YJ, Cao RR, et al. Triboelectric polymer with excellent enhanced electrical output performance over a wide temperature range. *Nano Energy.* 2023;110:108347.
122. Wang KQ, Li JJ, Li JF, et al. Hexadecane-containing sandwich structure based triboelectric nanogenerator with remarkable performance enhancement. *Nano Energy.* 2021;87:106198.
123. Zhang JJ, Zheng YB, Xu L, Wang DA. Oleic-acid enhanced triboelectric nanogenerator with high output performance and wear resistance. *Nano Energy.* 2020;69:104435.
124. Wang KQ, Wu CY, Zhang HL, Li JF, Li JJ. Cylindrical bearing inspired oil enhanced rolling friction based nanogenerator. *Nano Energy.* 2022;99:107372.
125. Zhou LL, Liu D, Zhao ZH, et al. Simultaneously enhancing power density and durability of sliding-mode triboelectric nanogenerator via interface liquid lubrication. *Adv Energy Mater.* 2020;10:2002920.
126. Zhang PP, Chen YH, Guo ZH, Guo WB, Pu X, Wang ZL. Stretchable, transparent, and thermally stable triboelectric nanogenerators based on solvent-free ion-conducting elastomer electrodes. *Adv Funct Mater.* 2020;30:1909252.
127. Xie XK, Zhang Y, Chen C, et al. Frequency-independent self-powered sensing based on capacitive impedance matching effect of triboelectric nanogenerator. *Nano Energy.* 2019;65:103984.
128. Wang TY, Li XF, Liu SM, et al. Self-assembled wide bandgap nanocoatings enabled outstanding dielectric characteristics in the sandwich-like structure polymer composites. *Nano Converg.* 2022;9:55.
129. Gao C, Liu T, Luo B, et al. Cellulosic triboelectric materials for stable energy harvesting from hot and humid conditions. *Nano Energy.* 2023;111:108426.
130. Zhao JM, Zhang WL, Liu T, et al. Hierarchical porous cellulosic triboelectric materials for extreme environmental conditions. *Small Methods.* 2022;6:2200664.
131. Hillmyer MA. The promise of plastics from plants. *Science.* 2017;358:868-870.
132. Gao D, Lv J, Lee PS. Natural polymer in soft electronics: opportunities, challenges, and future prospects. *Adv Mater.* 2022;34:2105020.
133. Li K, Wang SN, Chen H, Yang X, Berglund LA, Zhou Q. Self-densification of highly mesoporous wood structure into a strong and transparent film. *Adv Mater.* 2020;32:2003653.
134. Guan QF, Yang HB, Han ZM, Ling ZC, Yu SH. An all-natural bioinspired structural material for plastic replacement. *Nat Commun.* 2020;11:5401.
135. Wei ZT, Wang JL, Liu YH, et al. Sustainable triboelectric materials for smart active sensing systems. *Adv Funct Mater.* 2022;32:2208277.
136. Qin Y, Zhang WL, Liu YH, et al. Cellulosic gel-based triboelectric nanogenerators for energy harvesting and emerging applications. *Nano Energy.* 2023;106:108079.
137. Li Y, Wei CH, Jiang Y, et al. Continuous preparation of chitosan-based self-powered sensing fibers recycled from wasted materials for smart home applications. *Adv Fiber Mater.* 2022;4:1584-1594.
138. Tu H, Zhu MX, Duan B, Zhang LN. Recent progress in high-strength and robust regenerated cellulose materials. *Adv Mater.* 2021;33:2000682.
139. Shao YZ, Luo B, Liu T, et al. Harvesting energy from extreme environmental conditions with cellulosic triboelectric materials. *Mater Today.* 2023;66:348-370.

140. Cheng Z, Li JP, Wang B, et al. Comparative study on properties of nanocellulose derived from sustainable biomass resources. *Cellulose*. 2022;29:7083-7098.
141. Shen ZH, Qin ML, Xiong F, Zou RQ, Zhang J. Nanocellulose-based composite phase change materials for thermal energy storage: status and challenges. *Energy Environ Sci*. 2023;16:830-861.
142. Wang R, Ma JM, Ma S, et al. A biodegradable cellulose-based flame-retardant triboelectric nanogenerator for fire warning. *Chem Eng J*. 2022;450:137985.
143. Huang WJ, Wang YX, Huang ZQ, et al. On-demand dissolvable self-healing hydrogel based on carboxymethyl chitosan and cellulose nanocrystal for deep partial thickness burn wound healing. *ACS Appl Mater Interfaces*. 2018;10(48):41076-41088.
144. Su YJ, Yang TN, Zhao X, et al. A wireless energy transmission enabled wearable active acetone biosensor for non-invasive prediabetes diagnosis. *Nano Energy*. 2020;74:104941.
145. Šutka A, Linarts A, Mālnieks K, Stiprais K, Lapčinskis L. Dramatic increase in polymer triboelectrification by transition from a glassy to rubbery state. *Mater Horiz*. 2020;7:520-523.
146. Baytekin HT, Baytekin B, Hermans TM, Kowalczyk B, Grzybowski BA. Control of surface charges by radicals as a principle of antistatic polymers protecting electronic circuitry. *Science*. 2013;341:1368-1371.
147. Tsaia PP, Schreuder-Gibson H, Gibson P. Different electrostatic methods for making electret filters. *J Electrostat*. 2002;54:333-341.
148. Šutka A, Mālnieks K, Lapčinskis L, et al. The role of intermolecular forces in contact electrification on polymer surfaces and triboelectric nanogenerators. *Energy Environ Sci*. 2019;12:2417-2421.
149. Sohn A, Lee JH, Yoon H-J, Lee HH, Kim S-W. Self-boosted power generation of triboelectric nanogenerator with glass transition by friction heat. *Nano Energy*. 2020;74:104840.
150. Behl M, Razzaq MY, Lendlein A. Multifunctional shape-memory polymers. *Adv Mater*. 2010;22:3388-3410.
151. Zhang CL, Hu JL, Chen SJ, Ji FL. Theoretical study of hydrogen bonding interactions on MDI-based polyurethane. *J Mol Model*. 2010;16:1391-1399.
152. Niu SM, Wang SH, Lin L, et al. Theoretical study of contact-mode triboelectric nanogenerators as an effective power source. *Energy Environ Sci*. 2013;6:3576-3583.
153. Cheng L, Xu Q, Zheng YB, Jia XF, Qin Y. A self-improving triboelectric nanogenerator with improved charge density and increased charge accumulation speed. *Nat Commun*. 2018;9:3773.
154. Graham SA, Chandrarathna SC, Patnam H, Manchi P, Lee J-W, Yu JS. Harsh environment-tolerant and robust triboelectric nanogenerators for mechanical-energy harvesting, sensing, and energy storage in a smart home. *Nano Energy*. 2021;80:105547.
155. Rodrigues C, Kumar M, Proenca MP, et al. Triboelectric energy harvesting in harsh conditions: temperature and pressure effects in methane and crude oil environments. *Nano Energy*. 2020;72:104682.
156. Luo XX, Zhu LP, Wang Y-C, Li JY, Nie JJ, Wang ZL. A flexible multifunctional triboelectric nanogenerator based on MXene/PVA hydrogel. *Adv Funct Mater*. 2021;31:2104928.
157. Guo ZH, Wang HL, Shao JJ, et al. Bioinspired soft electroreceptors for artificial precontact somatosensation. *Sci Adv*. 2022;8:eabo5201.
158. Wang HL, Guo ZH, Zhu G, Pu X, Wang ZL. Boosting the power and lowering the impedance of triboelectric nanogenerators through manipulating the permittivity for wearable energy harvesting. *ACS Nano*. 2021;15(4):7513-7521.
159. Chen HM, Xu Y, Zhang JS, Wu WT, Song GF. Enhanced stretchable graphene-based triboelectric nanogenerator via control of surface nanostructure. *Nano Energy*. 2019;58:304-311.
160. Han JK, Yang JK, Gao WW, Bai H. Ice-templated, large-area silver nanowire pattern for flexible transparent electrode. *Adv Funct Mater*. 2021;31:2010155.
161. Liang XP, Li HF, Dou JX, et al. Stable and biocompatible carbon nanotube ink mediated by silk protein for printed electronics. *Adv Mater*. 2020;32:2000165.
162. Qi JB, Wang AC, Yang WF, et al. Hydrogel-based hierarchically wrinkled stretchable nanofibrous membrane for high performance wearable triboelectric nanogenerator. *Nano Energy*. 2020;67:104206.
163. Dong L, Wang MX, Wu JJ, Zhu CH, Shi J, Morikawa H. Stretchable, adhesive, self-healable, and conductive hydrogel-based deformable triboelectric nanogenerator for energy harvesting and human motion sensing. *ACS Appl Mater Interfaces*. 2022;14(7):9126-9137.
164. Xu W, Huang L-B, Wong M-C, Chen L, Bai GX, Hao JH. Environmentally friendly hydrogel-based triboelectric nanogenerators for versatile energy harvesting and self-powered sensors. *Adv Energy Mater*. 2017;7:1601529.
165. Chen ZS, Yu JH, Zeng HZ, et al. An electret/hydrogel-based tactile sensor boosted by micro-patterned and electrostatic promoting methods with flexibility and wide-temperature tolerance. *Micromachines*. 2021;12:1462.
166. Bao DQ, Wen Z, Shi JH, et al. An anti-freezing hydrogel based stretchable triboelectric nanogenerator for biomechanical energy harvesting at sub-zero temperature. *J Mater Chem A*. 2020;8:13787-13794.
167. Wang Y, Zhang LN, Lu A. Highly stretchable, transparent cellulose/PVA composite hydrogel for multiple sensing and triboelectric nanogenerators. *J Mater Chem A*. 2020;8:13935-13941.
168. Chen YZ, Shi CS, Zhang JF, et al. Ionic thermoelectric effect inducing cation-enriched surface of hydrogel to enhance output performance of triboelectric nanogenerator. *Energy Technol*. 2022;10:2200070.
169. Sun HL, Zhao Y, Jiao SL, et al. Environment tolerant conductive nanocomposite organohydrogels as flexible strain sensors and power sources for sustainable electronics. *Adv Funct Mater*. 2021;31:2101696.
170. Dai XY, Huang LB, Sun ZH, et al. A phonic Braille recognition system based on a self-powered sensor with self-healing ability, temperature resistance, and stretchability. *Mater Horiz*. 2022;9:2603-2612.
171. Huang L-B, Dai XY, Sun ZH, et al. Environment-resisted flexible high performance triboelectric nanogenerators based on ultrafast self-healing non-drying conductive organohydrogel. *Nano Energy*. 2021;82:105724.
172. Wu YH, Qu JK, Zhang XH, et al. Biomechanical energy harvesters based on ionic conductive organohydrogels via the

- Hofmeister effect and electrostatic interaction. *ACS Nano*. 2021;15(8):13427-13435.
173. Khan A, Ginnaram S, Wu C-H, et al. Fully self-healable, highly stretchable, and anti-freezing supramolecular gels for energy-harvesting triboelectric nanogenerator and self-powered wearable electronics. *Nano Energy*. 2021;90:106525.
 174. Xu S, Zhou ZD, Liu ZS, Sharma P. Concurrent stiffening and softening in hydrogels under dehydration. *Sci Adv*. 2023;9(1):eade3240.
 175. Guo X, Dong XY, Zou GJ, Gao HJ, Zhai W. Strong and tough fibrous hydrogels reinforced by multiscale hierarchical structures with multimechanisms. *Sci Adv*. 2023;9(2):eadf7075.
 176. Zhao YQ, Yang N, Chu X, et al. Wide-humidity range applicable, anti-freezing, and healable zwitterionic hydrogels for ion-leakage-free iontronic sensors. *Adv Mater*. 2023;35(22):2211617.
 177. Zhang ER, Bai RB, Morelle XP, Suo ZG. Fatigue fracture of nearly elastic hydrogels. *Soft Matter*. 2018;14:3563-3571.
 178. Cao ZQ, Liu HL, Jiang L. Transparent, mechanically robust, and ultrastable ionogels enabled by hydrogen bonding between elastomers and ionic liquids. *Mater Horiz*. 2020;7:912-918.
 179. Wang MX, Zhang PY, Shamsi M, et al. Tough and stretchable ionogels by in situ phase separation. *Nat Mater*. 2022;21:359-365.
 180. Shi L, Jia K, Gao YY, et al. Highly stretchable and transparent ionic conductor with novel hydrophobicity and extreme-temperature tolerance. *Research*. 2020;2020:2505619.
 181. Tang SM, Sha DY, He ZR, et al. Environmentally adaptable organo-ionic gel-based electrodes for real-time on-skin electrocardiography monitoring. *Adv Healthcare Mater*. 2023;12(18):2300475.
 182. Kim HJ, Chen BH, Suo ZG, Hayward RC. Ionoelastomer junctions between polymer networks of fixed anions and cations. *Science*. 2020;367(6479):773-776.
 183. Li QN, Liu ZY, Zheng SJ, et al. Three-dimensional printable, highly conductive ionic elastomers for high-sensitivity iontronics. *ACS Appl Mater Interfaces*. 2022;14(22):26068-26076.
 184. Liao WQ, Liu XK, Li YQ, et al. Transparent, stretchable, temperature-stable and self-healing ionogel-based triboelectric nanogenerator for biomechanical energy collection. *Nano Res*. 2022;15:2060-2068.
 185. Li HL, Xu FC, Guan TT, Li Y, Sun JQ. Mechanically and environmentally stable triboelectric nanogenerator based on high-strength and anti-compression self-healing ionogel. *Nano Energy*. 2021;90:106645.
 186. Sun LJ, Chen S, Guo YF, et al. Ionogel-based, highly stretchable, transparent, durable triboelectric nanogenerators for energy harvesting and motion sensing over a wide temperature range. *Nano Energy*. 2019;63:103847.
 187. Lu CW, Wang XY, Shen Y, et al. Liquid-free, anti-freezing, solvent-resistant, cellulose-derived ionic conductive elastomer for stretchable wearable electronics and triboelectric nanogenerators. *Adv Funct Mater*. 2022;32:2207714.
 188. Zhang KM, Chen S, Chen YL, et al. Elastomeric liquid-free conductor for iontronic devices. *Langmuir*. 2022;38(39):11994-12004.
 189. Cuce E, Cuce PM, Wood CJ, Riffat SB. Toward aerogel based thermal superinsulation in buildings: a comprehensive review. *Renew Sustain Energy Rev*. 2014;34:273-299.
 190. Feng JZ, Su BL, Xia HS, et al. Printed aerogels: chemistry, processing, and applications. *Chem Soc Rev*. 2021;50:3842-3888.
 191. Zhao SY, Malfait WJ, Guerrero-Alburquerque N, Koebel MM, Nyström G. Biopolymer aerogels and foams: chemistry, properties, and applications. *Angew Chem Int Ed*. 2018;57:7580-7608.
 192. Maleki H. Recent advances in aerogels for environmental remediation applications: a review. *Chem Eng J*. 2016;300:98-118.
 193. Wei G, Zhang JM, Usuelli M, Zhang XF, Liu B, Mezzenga R. Biomass vs inorganic and plastic-based aerogels: structural design, functional tailoring, resource-efficient applications and sustainability analysis. *Prog Mater Sci*. 2022;125:100915.
 194. He HL, Liu JR, Wang YS, et al. An ultralight self-powered fire alarm e-textile based on conductive aerogel fiber with repeatable temperature monitoring performance used in firefighting clothing. *ACS Nano*. 2022;16(2):2953-2967.
 195. Qian ZC, Li R, Guo J, et al. Triboelectric nanogenerators made of polybenzazole aerogels as fire-resistant negative tribo-materials. *Nano Energy*. 2019;64:103900.
 196. Yang Y, Zhang H, Liu R, Wen X, Hou T-C, Wang ZL. Fully enclosed triboelectric nanogenerators for applications in water and harsh environments. *Adv Energ Mater*. 2013;3:1563-1568.
 197. Zhang W, Hu Y, Ge J, Jiang HL, Yu SH. A facile and general coating approach to moisture/water-resistant metal-organic frameworks with intact porosity. *J Am Chem Soc*. 2014;136(49):16978-16981.
 198. Hu LG, Wu WH, Gong L, et al. A novel aluminum-based metal-organic framework with uniform micropores for trace BTEX adsorption. *Angew Chem Int Ed*. 2023;62:e202215296.
 199. Li SL, Wang TN, Tang D, et al. Metal-organic framework integrating ionic framework and bimetallic coupling effect for highly efficient oxygen evolution reaction. *Adv Sci*. 2022;9:2203712.
 200. Wang JW, Qiao LZ, Nie HD, et al. Facile electron delivery from graphene template to ultrathin metal-organic layers for boosting CO₂ photoreduction. *Nat Commun*. 2021;12:813.
 201. Chong S, Thiele G, Kim J. Excavating hidden adsorption sites in metal-organic frameworks using rational defect engineering. *Nat Commun*. 2017;8:1539.
 202. Wen LL, Sun K, Liu XS, Yang WJ, Li LY, Jiang HL. Electronic state and microenvironment modulation of metal nanoparticles stabilized by MOFs for boosting electrocatalytic nitrogen reduction. *Adv Mater*. 2023;35(13):2210669.
 203. Kaye SS, Dailly A, Yaghi OM, Long JR. Impact of preparation and handling on the hydrogen storage properties of Zn₄O(1,4-benzenedicarboxylate)₃ (MOF-5). *J Am Chem Soc*. 2007;129(46):14176-14177.

How to cite this article: Cao R, Liu Y, Li H, et al. Advances in high-temperature operatable triboelectric nanogenerator. *SusMat*. 2024;4:e196. <https://doi.org/10.1002/sus2.196>

AUTHOR BIOGRAPHIES



Ruirui Cao is currently an associate Professor in the School of Future Technology and Henan Key Laboratory of Photovoltaic Materials at Henan University. She received her Ph.D. from School of Material Science and Engineering of Tiangong University in 2019 and

then joined the Henan Key Laboratory of Photovoltaic Materials, Henan University. Her research focuses on energy conversion and storage, self-powered sensing, and flexible electronic devices.



Chong Chen is now a senior research fellow at Hefei Institute of Physical Science (HIPS), Chinese Academy of Sciences (CAS). He received his Ph.D. degree from Institute of Plasma Physics, CAS in 2009. Subsequently he moved to Korea Advanced Institute of Sci-

ence and Technology (South Korea) and South Dakota State University (SA), as a postdoctoral fellow, respectively. From 2012 to 2022, he worked as a distinguished professor at Henan University. He has been a senior research fellow at HIPS under the CAS since 2023 and is leading a group that mainly studies photovoltaic materials and thin film solar cells.



Caofeng Pan received his B.S. degree (2005) and his Ph.D. (2010) in Materials Science and Engineering from Tsinghua University, China. He then joined the Georgia Institute of Technology as a postdoctoral fellow. He is currently a professor and a group leader at

Beijing Institute of Nanoenergy and Nanosystems, Chinese Academy of Sciences since 2013. His main research interests focus on the fields of low dimensional materials for fabricating smart electronic and optoelectronic devices for tactile sensing.